Developing aTranswell Millifluidic Device for Studying Blood-Brain Barrier Endothelium

Journal:	*Lab on a Chip*
Manuscript ID	LC-ART-07-2022-000657.R2
Article Type:	Paper
Date Submitted by the Author:	08-Oct-2022
Complete List of Authors:	Harding, Ian; Northeastern University College of Engineering, Department of Bioengineering O'Hare, Nicholas; Northeastern University College of Engineering, Department of Chemical Engineering Vigliotti, Mark; Northeastern University College of Engineering, Department of Chemical Engineering Caraballo, Alex ; Northeastern University College of Engineering, Department of Chemical Engineering Lee, Claire; Northeastern University College of Engineering, Department of Bioengineering Millican, Karina ; Northeastern University College of Engineering, Department of Bioengineering Herman, Ira; Tufts University Sackler School of Graduate Biomedical Sciences, Department of Developmental, Molecular, and Chemical Biology; Tufts University Sackler School of Graduate Biomedical Sciences, Center for Innovations in Wound Healing Research Ebong, Eno; Northeastern University College of Engineering, Department of Chemical Engineering; Northeastern University College of Engineering, Department of Bioengineering; Albert Einstein College of Medicine, Department of Neuroscience

Developing a Transwell Millifluidic Device for Studying Blood-Brain Barrier Endothelium

Ian C. Harding[1,6], Nicholas R. O'Hare[2,6], Mark Vigliotti[2], Alex Caraballo[2], Claire I. Lee[1], Karina Millican[1], Ira M. Herman[3,4], Eno E. Ebong[1,2,5]

[1]Department of Bioengineering, Northeastern University, Boston, MA, USA
[2]Department of Chemical Engineering, Northeastern University, Boston, MA, USA
[3]Department of Developmental, Molecular, and Chemical Biology, Tufts School of Graduate Biomedical Sciences, Boston, MA, USA
[4]Center for Innovations in Wound Healing Research, Tufts University School of Medicine, Boston, MA, USA
[5]Department of Neuroscience, Albert Einstein College of Medicine, New York, NY, USA
[6]These authors made equal contributions to this work.

October 24, 2022

Correspondence:
Eno E. Ebong, Ph.D.
Department of Chemical Engineering
Northeastern University
360 Huntington Avenue
129 Interdisciplinary Science and Engineering Complex
Boston, MA, 02115
Phone: 617-373-8744
Fax: 617-373-2209
Emails: e.ebong@northeastern.edu

Running Foot: "Millifluidic Blood-Brain Barrier Device"

ABSTRACT

Blood-brain barrier (BBB) endothelial cell (EC) function depends on flow conditions and on supportive cells, like pericytes and astrocytes, which have been shown to be both beneficial and detrimental for brain EC function. Most studies investigating BBB EC function lack physiological relevance, using sub-physiological shear stress magnitudes and/or omitting pericytes and astrocytes. In this study, we developed a millifluidic device compatible with standard transwell inserts to investigate BBB function. In contrast to standard polydimethylsiloxane (PDMS) microfluidic devices, this model allows for easy, reproducible shear stress exposure without common limitations of PDMS devices such as inadequate nutrient diffusion and air bubble formation. In no-flow conditions, we first used the device to examine the impact of primary human pericytes and astrocytes on human brain microvascular EC (HBMEC) barrier integrity. Astrocytes, pericytes, and a 1:1 ratio of both cell types increased HBMEC barrier integrity via reduced 3- and 40-kDa fluorescent dextran permeability and increased claudin-5 expression. There were differing levels of low 3-kDa permeability in HBMEC-pericyte, HBMEC-astrocyte, and HBMEC-astrocyte-pericyte co-cultures, while levels of low 40-kDa permeability were consistent across co-cultures. The 3-kDa findings suggest that pericytes provide more barrier support to the BBB model compared to astrocytes, although both supportive cell types are permeability reducers. Incorporation of 24-hour 12 dynes/cm^2 flow significantly reduced dextran permeability in HBMEC monolayers, but not in the tri-culture model. These results indicate that tri-culture may exert more pronounced impact on overall BBB permeability than flow exposure. In both cases, monolayer and tri-culture, flow exposure interestingly reduced HBMEC expression of both claudin-5 and occludin. ZO-1 expression, and localization at cell-cell junctions increased in the tri-culture but exhibited no apparent change in the HBMEC monolayer. Under flow conditions, we also observed HBMEC alignment in the tri-culture but not in HBMEC monolayers, indicating supportive cells and flow are both essential to observe brain EC alignment in vitro. Collectively, these results support the necessity of physiologically relevant, multicellular BBB models when investigating BBB EC function. Consideration of the roles of shear stress and supportive cells within the BBB is critical for elucidating the physiology of the neurovascular unit.

Key Words: blood-brain barrier, endothelial cells, astrocytes, pericytes, shear stress, mechanotransduction

INTRODUCTION

Neurological disorders are the second leading cause of death worldwide and the leading cause of daily-adjusted life years, a sum of the years of potential life lost and the years of productive life lost[1]. Over the past several decades, numerous studies have identified correlations between many neurological disorders, such as Alzheimer's[2-5], stroke[6-8], multiple sclerosis[9-11], traumatic brain injury[12-14], and dysfunction of the blood-brain barrier (BBB), a complex, multicellular structure composed of endothelial cells (ECs), pericytes (PCs), astrocytes (ACs), (**Figure 1a**)[15, 16]. These studies, among others, suggest that BBB dysfunction in neurological disorders may even contribute to their pathology. Therefore, identifying the regulatory mechanisms of BBB integrity may provide therapeutic targets for neurological disorders.

Proper function of the BBB requires constant communication between brain endothelial cells (ECs) and supportive cells such as PCs, ACs, neurons, and microglia. Although neurons and microglia may be implicated in BBB integrity, their relevance to overall function is much more ambiguous thus they will not be included in the model. PCs and ACs have been shown to regulate the expression of endothelial transporters and tight junction proteins, thereby promoting reduced permeability within the BBB[17-22]. For example, the addition of PCs and ACs to brain EC monolayers has been shown to increase the expression of the tight junction proteins zona occludins-1 (ZO-1), claudin-5, and occludin[23-25]. Supportive PCs and ACs have also been shown to impact EC caveolin-1[26], implicated in endocytosis, and the adherens junction protein VE-cadherin[27], although this has been less studied. While many studies have identified beneficial roles of ACs and PCs in BBB function, others have found contradicting results, including in diseased states[28-31]. Thus, the relationship between ECs and neighboring PCs and ACs is not clear and needs to be elucidated.

Brain EC exposure to shear stress has also been shown to improve barrier integrity[32-36]. For instance, Colgan *et al.* found that the application of shear stress at a rate of 14 dynes/cm^2 reduces permeability and increases the expression of ZO-1 and claudin-5. However, this study utilized bovine brain ECs, limiting its physiological relevance. Other studies have similarly investigated the relationship between shear stress and function of brain ECs and BBB, but typically use non-human and/or immortalized ECs[34, 37], apply sub-physiological shear stress magnitudes[32, 33], or fail to include relevant supportive cells including PCs and ACs[32-36, 38]. The use of immortalized ECs, for example, is essential for their development as a research and therapeutic tool. However, they are limited by lower TEER values, higher permeability, and questionable tight junction protein expression [39-41] and do not presently achieve the degree of physiological relevance that primary ECs achieve. Sub-physiological shear stress is an issue because brain ECs resist elongation and alignment in the direction of shear stress, a classical endothelial response to fluid flow that is exhibited by ECs from other vascular beds. Lastly, for the reasons described in the above paragraph, absence of PCs and ACs limits the conclusions that can be derived from some prior studies of the effect of shear stress on BBB integrity.

Early multicellular, *in vitro* BBB models were typically cultured on transwell inserts and maintained in static conditions[23, 42-46]. These models thus had limited physiological relevance due to a lack of shear stress created by fluid flow. Therefore, with advances in microfluidic research, static BBB models were adapted to microfluidic formats, most commonly via the use of polydimethylsiloxane (PDMS)[47-50]. However, despite the advances and successful applications of PDMS-based microfluidic BBB models, they are often complicated by issues of nutrient depletion, absorption of small molecules into the substrate, and fabrication difficulties[51-53]. Most microfluidic

3

devices thus require sufficient expertise to utilize. Although transwell-compatible microfluidic devices have recently been developed, they still require soft lithography experience while our model does not[54]. A comparable system known as DynaMiTES has also been investigated although non-physiological shear stress may limit its viability for BBB modeling [55, 56]. Therefore, a need exists to develop a multicellular BBB model that applies physiological fluid flow and overcomes the challenges associated with common PDMS microfluidics and soft lithography.

The goal of this study was to develop an easy-to-use BBB fluidic model that overcomes common limitations of previous models such as issues with nutrient diffusion and the use of immortalized cell lines or non-human primary cells **(Figure 1b)**. Using this device, we could then clarify previously confounding results regarding the impacts of PCs and ACs on BBB phenotype while also further identifying the impact of flow on BBB integrity. To achieve these goals, we first established a physiologically relevant BBB model in transwell inserts consisting of primary human brain microvascular endothelial cells (HBMECs), human PCs, and human ACs. This transwell model was incorporated into a custom millifluidic device to allow for the application of physiological levels of shear stress while maintaining the device's ease of use and compatibility with downstream analytical molecular biology techniques. The impact of PC and AC addition and shear stress exposure were subsequently analyzed via dextran permeability assays, cell alignment, and the expression of permeability-regulating proteins via western blotting and immunocytochemistry. We hypothesized that a physiologically relevant, BBB model could be obtained using the proposed multicellular, millifluidic system. With the model, we speculated that astrocytes and pericytes would have a compounding effect on BBB integrity while increasing key tight junction protein expression. Additionally, we postulated that uniform flow exposure would decrease permeability through an upregulation of tight junctions.

MATERIALS & METHODS

Cell Culture

HBMECs were purchased from Cell Systems (Kirkland, WA) and used between passages 6 and 8. Cells were cultured in Endothelial Cell Growth Media MV2 from PromoCell (Heidelberg, Germany) supplemented with penicillin-streptomycin (100 U/mL and 100 μg/mL, respectively) and the MV2 SupplementPack, which includes fetal calf serum (0.05 mL/mL), recombinant human epithelial growth factor (5 ng/mL), recombinant human basic fibroblast growth factor (10 ng/mL), insulin-like growth factor (20 ng/mL), recombinant human vascular endothelial growth factor 165 (0.5 ng/mL), ascorbic acid (1 μg/mL), and hydrocortisone (0.2 μg/mL). Primary human brain vascular PCs were purchased from ScienCell (Carlsbad, CA) and used between passages 3 and 6. Cells were cultured in ScienCell Pericyte Medium supplemented with fetal bovine serum (0.02 mL/mL), pericyte growth supplement (0.01 mL/mL), and penicillin-streptomycin (100 U/mL and 100 μg/mL, respectively). Primary human ACs isolated from the cerebral cortex were purchased from ScienCell (Carlsbad, CA) and used between passages 4 and 7. Cells were cultured in ScienCell Astrocyte Medium supplemented with fetal bovine serum (0.02 mL/mL), astrocyte growth supplement (0.01 mL/mL), and penicillin-streptomycin (100 U/mL and 100 μg/mL, respectively). Cell culture flasks for PCs and ACs were coated with poly-L-lysine (2 μg/cm^2 in water) for at least 1 hour and up to 24 hours prior to being plated with PCs and ACs. In addition to HBMEC, PC, and AC cell cultures, human aortic endothelial cells (HAECs) acquired from PromoCell (Heidelberg, Germany) were also utilized to validate flow patterns generated by the millifluidic device. HAECs were similarly cultured in PromoCell Endothelial Cell Growth Media MV2 as previously described. All cell types were cultured in a humidified incubator maintained at 37°C and 5% CO_2.

Transwell Blood-Brain Barrier Model Development

A BBB model containing HBMECs, PCs, and ACs was developed using 24-well transwell inserts (Falcon®) (**Figure 1c,d**). To develop the model, 5 x 10^5 HBMECs were first plated on the 0.33 cm^2 area of the abluminal side of inverted, fibronectin-coated (15 μg/cm^2) transwell insert membranes (HBMEC plating density of 1.5 x 10^6 cells/cm^2). The inverted transwell inserts were then placed into a humidified incubator at 37°C and 5% CO_2 for one hour to allow for cell attachment. Following the one-hour incubation period, the transwell inserts were then inverted to their right-side-up positions and placed into the wells of 24-well plates containing 700 μL of PromoCell MV2 media. At this time, 5 x 10^5 PCs and 5 x 10^5 ACs were plated onto the luminal side of transwell insert membranes in the absence of a fibronectin coating and covered with 300 μL of ScienCell media (150 μL of each PC and AC media). Cells were then placed into the incubator and allowed to grow for 3-4 days with media changes taking place every other day. The chosen seeding densities were utilized to obtain an approximate 1:1:1 ratio of HBMECs:PCs:ACs upon cell confluency. In addition to the HBMEC/PC/AC co-culture BBB model, HBMEC monoculture, HBMEC/PC co-culture, and HBMEC/AC co-culture models were also developed to determine both the impact of PCs versus ACs on HBMEC phenotype and the impact of shear stress on HBMEC monolayers. These models were developed as described above but with either no cells on the luminal membrane or only one cell type (either PCs or ACs) on the luminal membrane. It should also be noted that for static dextran permeability assays the BBB cell organization was revised from what is described above, and revisions are described below where appropriate.

Design and Fabrication of Blood-Brain Barrier Millifluidic System

ECs of the above-described BBB model containing HBMECs, PCs, and ACs or HBMEC monolayers were exposed to a continuous, physiologically relevant shear stress of 12 dynes/cm^2 [57] for 24 hours using a custom, transwell-compatible, millifluidic device as detailed below. While previous BBB microfluidics, which are commonly made out of PDMS, are often limited by issues of nutrient diffusion and air bubble formation; the use of immortalized cell lines or non-human primary cells; and a lack of adaptability for downstream analytical techniques such as high magnification fluorescence microscopy [47-50, 58-61], this device overcomes these limitations due to its compatibility with the transwell inserts, which have been utilized for decades to study BBB function[15, 23, 42-46]. The transwell millifluidic device was fabricated out of acrylic and designed using SolidWorks (**Figure 1b**). The device follows the basic format of parallel-plate flow chambers with a chamber bottom, chamber top, and silicone gasket to prevent leakage, but was designed to be compatible with 24-well transwell inserts. The flow channel within the device measures 75x13x0.5 mm (L x W x H) (**Figure 1b**). Further dimensions of the device are described in U.S. Patent Application No. 17/454,768 that has been filed**.** To assemble the device, a transwell insert was placed into the top of the millifluidic device, which contains precisely designed notches to allow for the transwell membrane to align flush with the flow channel. The chamber top was then attached to the chamber bottom, with a silicone gasket in between to prevent leakage, using screws. A lid and additional silicone gasket were then secured directly above the transwell insert to prevent leakage from this orifice. 70 mL of media was added to the system, which included a media reservoir (with 10-20 mL of media) for CO_2 diffusion, a pulse dampener (with less than 10 mL of media) to reduce flow pulsatility, and the rest of the flow loop (with just over 40 mL of media) consisting of tubing and the millifluidic device **(Supplemental Figure 1)**. The system was then connected to a peristaltic pump to drive and recirculate the flowing media. The flow patterns and shear stress magnitudes that were generated were validated via SolidWorks Flow Simulation. A shear stress of 12 dynes/cm^2 was selected as the reasonable starting point for our first-generation BBB model based on previous studies providing a wide range of shear stresses to apply when modeling human brain microvasculature. Some of the previous work is summarized in **Supplemental Table 1**. We also selected 12 dynes/cm^2 based on our own prior experience and so that we can incorporate the HAECs in our validation of our BBB model. Our future work will investigate a wider range of shear stresses to identify optimal shear stress conditions for recapitulating brain microvasculature physiology and pathology. During shear stress exposure, the flow system, with the exception of the peristaltic pump, was contained within a humidified incubator at 37°C and 5% CO_2 **(Supplemental Figure 1).**

Live Fluorescent Particle Tracking for Millifluidic Validation

To confirm flow patterns within the transwell millifluidic device, live tracking of fluorescent particles was performed. Specifically, fluorescent polystyrene microspheres (Bangs Laboratories; Fishers, IN) with an average diameter of 1 μm were diluted in water at a 1:1000 dilution, which was then perfused through the millifluidic device. Particle movement was subsequently tracked via the use of a Zeiss Axio Observer Z1 fluorescent microscope.

HBMEC Flow Exposure Using a Previously Fabricated Parallel Plate Flow Chamber

In addition to the transwell millifluidic, a previously fabricated parallel plate flow chamber was also utilized, particularly to investigate the impact of flow on HBMEC alignment. This device is based on a modified parallel plate flow chamber adapted from previous work[62]. For these

experiments, HBMECs were plated on fibronectin-coated (15 µg/cm²) glass coverslips and incorporated into the flow chamber for 24 hours of shear stress exposure at 12 dynes/cm².

Dextran Permeability Assay for Cell Culture Studies

To assess the mono- and co-culture systems for barrier function, a dextran permeability assay using Texas Red-conjugated 40 kDa dextran and 3 kDa dextran (Thermo Fisher; Waltham, MA) was performed. Assays were performed on cell culture models after 3-4 days of culture in static conditions. Customarily, such assays are performed to assess permeability from the luminal side of the transwell insert, with the apical side of the ECs facing the lumen of the transwell inserts and, therefore, permeability being measured from the apical side of the EC layer to the basal side of the EC layer. However, our flow-conditioning experiment dictated organization of HBMECs, PCs, and ACs as described above (**Figure 1c**), which meant that dextran permeability would be measured from the basal HBMEC side to the apical HBMEC side. For non-flow-conditioned samples, the organization of HBMECs, PCs, and ACs was reversed, with PCs and ACs plated on the abluminal transwell membrane surface while HBMECs were plated on the luminal surface (**Figure 1d**) as is customary, which meant that dextran permeability would be measured from the apical HBMEC side to the basal HBMEC side. Matching the flow-conditioned co-culture organization to the non-flow-conditioned co-culture organization was considered but deemed unnecessary, by checking for differences in measured permeability for the apical to basal vs. basal to apical configurations. Specifically, the 40 kDa dextran fluorescent intensity in media collected on the abluminal side was measured and results from both plating orientations were compared against each other (**Supplemental Figure 2a**). There was no apparent difference based on orientation of the cells, consistent with the findings of Hinkel et al. who performed a sodium fluorescein permeability assay[55].

For both static and flow-conditioned samples, 40 kDa dextran was added to the luminal transwell compartment at a concentration of 0.5 mg/mL in 200 µL of PromoCell MV2 medium. The same procedure was followed for the 3 kDa dextran except 0.25 mg/mL was added to the luminal compartment to conserve dextran. For flow conditioned samples, transwells were first removed from the millifluidic device and then placed in a fresh 24-well plate (or at least in fresh wells) for subsequent dextran permeability analysis. The static conditioned samples were also transferred to a fresh well/plate. The abluminal compartment was filled with 700 µL of the appropriate medium, depending on the model used (mono- or co-culture). Sixty minutes after the dextran was introduced to the system, 50µL of media from the abluminal compartment was collected. The collected media was analyzed for fluorescent dextran content using a Molecular Devices SpectraMax i3x plate reader. Dextran concentration within experimental samples was determined by comparison to fluorescent values obtained from a standard curve. The apparent permeability was then calculated using Equation 1:

$$P_{app} = \frac{C_a * V_a}{t * s * C_l} \quad (1)$$

where P_{app} is the apparent permeability, C_a is the measured abluminal dextran concentration, V_a is the abluminal media volume, t is time, s is surface area and C_l is the initial luminal dextran concentration. To determine the permeability coefficient of the BBB model independent of the porous transwell membrane, the permeability coefficient of a blank, fibronectin-coated transwell

membrane was determined. The permeability coefficient of the BBB model was then calculated using Equation 2:

$$\frac{1}{P_{app}} = \frac{1}{P_M} + \frac{1}{P_{BBB}} \quad (2)$$

where P_M is the permeability coefficient of the cell-free transwell membrane and P_{BBB} is the permeability coefficient of the BBB model. The derivation of the permeability equation was based on mass transport principles and aligns with previously described permeability studies [63-65].

Transepithelial Electrical Resistance for Cell Culture Studies

Transepithelial electrical resistance (TEER) of HBMECs monocultures was measured to assess barrier function. Before testing, proper media volumes in both the luminal (300μL) and abluminal (700μL) compartments were ensured. TEER was measured using a World Precision Instruments Epithelial Volt/Ohm Meter (EVOM2) and chopstick electrode. Three measurements for each sample were collected to provide increased accuracy. The average of the three measurements was used for statistical analysis.

Fluorescent Labeling of Target BBB Proteins

To ensure proper cell growth and phenotype within the BBB model, including EC monolayer formation and the presence of astrocyte foot processes, the BBB model was first evaluated using immunocytochemistry (ICC) via the following cell specific markers: platelet-EC adhesion molecule-1 (PECAM-1), neural/glial antigen 2 (NG2), and glial fibrillary acidic protein (GFAP) for HBMECs, PCs, and ACs, respectively. Additionally, HBMECs were also analyzed for junctional integrity via ICC of ZO-1 and claudin-5. Prior to ICC, at room temperature, cells to be labeled for PECAM-1, NG2, or GFAP were fixed in 4% paraformaldehyde for 20 minutes and subsequently permeabilized with 0.5% Triton X-100 for 5 minutes. Cells to be labeled for ZO-1 and claudin-5 were fixed and permeabilized in ice-cold methanol for 5 minutes at -20°C. Fixation and permeabilization steps were followed by blocking cells with 5% goat serum for 1 hour at room temperature. All samples were next incubated with the following primary antibodies diluted in blocking solution overnight at 4°C: rabbit anti-PECAM-1 (1:400; Novus Biologicals; Centennial, CO), mouse anti-NG2 (1:100; eBioscience; San Diego, CA), rat anti-GFAP (1:1,500; Invitrogen; Waltham, MA), rabbit anti-ZO-1 (1:200; Invitrogen; Waltham, MA), and mouse anti-claudin-5 (1:100; Invitrogen; Waltham, MA). Samples were incubated with the following secondary antibodies diluted in phosphate buffered saline for 1 hour at room temperature: goat anti-rabbit Alexa Fluor 647 (1:500; Invitrogen; Waltham, MA), goat anti-mouse Alexa Fluor 488 (1:500; Invitrogen; Waltham, MA), and goat anti-rat Alexa Fluor 546 (1:1,500; Invitrogen; Waltham, MA).

For ECs only, the cytoskeleton was also visualized. Cells were fixed in 4% paraformaldehyde for 10 minutes. Subsequently, 0.2% Triton X-100 was applied to permeabilize the cells before blocking non-specific staining sites with 3% goat serum combined with 0.2% Triton X-100. Lastly, the ECs were incubated with Alexa Fluor 594 conjugated F-actin phalloidin diluted in 3% BSA.

Additional BBB phenotyping was performed by using wheat germ agglutinin (WGA) lectin as a general stain for the HBMEC glycocalyx (GCX), which is a potential regulator of the cerebral vascular molecular permeability and charge barrier[66-68], although this function is understudied. For WGA staining, cells were fixed in 2% paraformaldehyde and 0.1% glutaraldehyde for 30 minutes at room temperature then blocked in 3% BSA for 30 minutes. Samples were incubated for 1 hour at room temperature using biotinylated WGA (1:100; Vector Labs; Burlingame, CA). Secondary labelling was performed for 30 minutes at room temperature using Alexa Fluor 488 conjugated streptavidin (1:500; Jackson ImmunoResearch; West Grove, PA).

After all fluorescent stains were completed, BBB membranes were removed from the transwells using a 6 mm biopsy punch and subsequently mounted on a microscope slide or placed in glass bottom petri dishes (Cellvis; Mountain View, CA) with a #0 coverslip thickness. Antifade mounting medium containing 4',6-Diamidine-2'-phenylindole (DAPI) dihydrochloride (Vector Labs, Burlingame, CA) was applied, to preserve the fluorescence while labeling cell nuclei. The samples were then sandwiched, between a 1 mm glass cover slide and the microscope slide or between a thin confocal slide and the glass bottom petri dish, before being sealed with nail polish. The sandwich was stored overnight for thorough diffusion of the mounting medium and DAPI before performing confocal imaging. Samples were imaged using a Zeiss LSM 880 confocal microscope with a 20x magnification dry lens or a 40x magnification water immersion lens objective.

Western Blotting

For western blot analysis, HBMECs cultured on the abluminal side of transwell membranes were lysed using radioimmunoprecipitation assay buffer containing 150 mM sodium chloride (NaCl), 1% Triton X-100, 50 mM Tris base, 0.1% sodium dodecyl sulfate (SDS), 5 mM ethylenediaminetetraacetic acid, 1 mM phenylmethylsuphonyl fluoride, and Roche cOmplete EDTA-free protease inhibitor cocktail. Prior to SDS polyacrylamide gel electrophoresis (SDS-PAGE), HBMEC protein lysates were prepared in Lamelli buffer containing 50 mM dithiothreitol and boiled at 95°C for 5 minutes. Protein lysates were then run on 7.5% SDS-PAGE gels and wet transferred to polyvinylidene difluoride (PVFD) membranes. It should be noted that the concentration of protein obtained from 0.33 cm^2 surface of the transwell inserts was low due to limited cell content. Therefore, to accommodate the subsequently low quantity of protein loaded on SDS-PAGE gels (~5 µg per well), a Pierce Western Blot Signal Enhancer was utilized following the manufacturer's protocol to amplify the signal of all proteins probed on the PVDF membranes except β-actin protein, which was utilized as a housekeeping protein. Membranes were blocked using 5% milk solution and probed with primary antibodies overnight at 4°C on a rocker at the following dilutions: ZO-1 (1:750; Invitrogen; Waltham, MA), occludin (1:1000; Invitrogen; Waltham, MA), claudin-5 (1:1000; Invitrogen; Waltham, MA), VE-cadherin (1:1000; BioLegend, San Diego, CA), caveolin-1 (1:1000; Santa Cruz Biotechonology; Dallas, TX), and B-actin (1:3,000; Invitrogen; Waltham, MA). These proteins were probed due to their implication in BBB permeability. All samples were incubated with species-appropriate, HRP-conjugated secondary antibodies for 1 hour at room temperature on a rocker at a 1:3,000 dilution in blocking buffer, except for β-actin, which utilized a 1:10,000 secondary antibody concentration. For chemiluminescent detection, samples were incubated in BioRad Clarity ECL reagents for 5 minutes at room temperature and imaged using a BioRad ChemiDoc Touch Imaging System.

Statistical Analysis

All data is presented as mean ± standard error of the mean. Prior to statistical analysis, western blot data was normalized to the housekeeping gene to account for loading differences and subsequently normalized to the control groups within each experiment to eliminate any confounding inter-experiment variables such as cell passage number. Normal distributions of data were confirmed using the Shapiro Wilk test. Subsequently, one-way ANOVAs with post-hoc Tukey's multiple comparison tests were used to identify statistically significant differences between groups. Alternatively, data from dextran permeability assays, specifically for flow-treated samples, was analyzed using a paired t-test to similarly remove bias introduced from inter-experiment variables.

RESULTS & DISCUSSION

Validation of the Transwell Millifluidic System

A millifluidic device compatible with commonly used 24-well Transwell inserts was designed to investigate the impact of shear stress exposure on BBB integrity (**Figure 1b**). The millifluidic follows the design of a standard parallel-plate flow chamber with a flow channel measuring 70x13x0.5 mm (L x W x H). Flow patterns and associated shear stresses were predicted via SolidWorks Flow Simulation (**Figure 1e**). Specifically, a flow rate of 72 mL/min generated a physiologically relevant shear stress of 12 dynes/cm^2. Live tracking of fluorescent microbeads was used as a first validation step, to ensure that flow patterns predicted by the computational model translated into practice (**Figure 1f**). As a second validation step, the system was scanned for the presence of microbubbles. No microbubble formation was observed during testing or use of the device.

As a third step in the validation of the Transwell Millifluidic System, we used the system to investigate the impact of shear stress application on EC alignment, a common EC mechanobiological response. In our review of previous studies, we did not see reported observations of brain EC alignment in the direction of flow[69-71]. In fact, some studies have highlighted the fact that brain EC resistance to elongation could be an evolutionary advantage due to decrease length of cell-cell junctions[15, 69]. Consistent with the previous reports, we observed that HBMECs cultured on the transwell membrane and exposed to 12 dynes/cm^2 of shear stress did not align in the direction of flow and may even exhibit perpendicular alignment **(Figure 2a)**. Therefore, to confirm proper flow patterns and resulting shear stresses within the transwell millifluidic device using cell alignment as an indicator, the device was tested using HAECs, which are well-characterized and known to align in the direction of flow exposure[72, 73]. Consistent with the literature, we found that HAECs did indeed align in the direction of flow after 24 hours of shear stress exposure at 12 dynes/cm^2 (**Figure2b**). These results validate the flow patterns and shear stresses predicted by the computational model.

Validation of BBB Model Embedded in the Transwell Millifluidic System

After validating proper function of the transwell millifluidic system via live tracking of fluorescent microbeads, by scanning for microbubbles, and by investigating cell alignment, attention was turned to the BBB model that would be embedded within the transwell millifluidic system.

The first step in validating the BBB model was focused on the brain ECs, which we **(Figure 2a)** and others[69-71] found to resist alignment in the direction of flow. We sought to close the gap in knowledge about how to stimulate brain EC alignment with flow. In pilot studies we probed alignment further, by using a previously fabricated, well-characterized, parallel-plate flow chamber in which the HBMECs were cultured on fibronectin-coated glass coverslips. This model was used for simplicity, and we acknowledge that the substrate on which cells are grown (glass coverslip vs. polycarbonate membrane) may also influence cells' alignment. We also varied the density at which the cells were plated on the glass coverslips, to compare the effects of low versus high cell densities before exposure to uniform flow. We found that resultant cell alignment parallel to the direction of flow did occur for HBMECs but depended on cell density at the time of flow introduction (**Supplemental Figure 3**). Cells exposed to flow at a lower cell density (~562 cells/mm^2) aligned in the direction of flow statistically significantly **Supplemental Figure 3**) when compared to static controls and consistent with previous studies on ECs from different

vascular beds. An average of 22.3 ± 1.0% of cells aligned within 15° of the axis parallel to flow while a similar amount are perfectly aligned with flow (**Supplemental Figure 3**). An average of 8.1 ± 0.6% of cells aligned within 15° of the axis perpendicular to flow while a similar amount are exactly perpendicular with flow (**Supplemental Figure 3**). Cells exposed to flow at a higher cell density (~1174 cells/mm^2) exhibited a decreased tendency to align with flow, which was statistically different (**Supplemental Figure 3**) from both static and low cell density uniform flow samples. In high cell density samples, only 18.4 ± 3.3% of cells aligned within 15° of the flow axis while 11.8 ± 2.2% of cells aligned within 15° of the axis perpendicular to flow (**Supplemental Figure 3**). The dependency of HBMEC alignment on cell density may be explained by the fact that EC migration rate is reduced at higher cell densities. Thus, cells at higher densities may require additional flow exposure time to adjust their configuration and achieve the same level of cell alignment. In addition, the fact that alignment of HBMECs depends on cell density while cell density is not a concern for successful HAEC alignment suggests that differences in alignment propensity exist between ECs of different vascular beds. However, the demonstration that HBMECs can indeed align in the direction of flow after 24 hours of exposure is new and valuable information given that several previous studies did not report brain EC alignment in the direction of flow. Furthermore, numerous studies have demonstrated alignment and barrier function to be dependent on a variety of other factors separate from shear stress including cell-cell interactions, substrate choice, cell density, and chemical/physical properties[18, 74-76]. Based on the current breadth of literature on HBMEC and HAEC alignment, these preliminary studies gave us the confidence to conduct the next steps in the validation of the transwell BBB millifluidic system utilizing HBMEC and not simply HAECs or other ECs that are not specific to the BBB.

Secondly, we sought to determine the ideal culture time of BBB constructs. For this step, the HBMECs were grown on the Transwell inserts until full confluence. While the monolayer was growing and reaching confluence, TEER of HBMEC monolayers was measured (**Figure 1g,h**). We found that HBMEC TEER increased from ~80 Ohms*cm^2 to ~97 Ohms*cm^2 over a three-day period and subsequently remained stable. Thus, all BBB models, which contained primary HBMECs, human PCs, and human ACs at an approximate 1:1:1 HBMEC:PC:AC ratio, were cultured for 3 or 4 days before experimentation. Additionally, the TEER of the HBMEC monolayer was compared between static and post-flow conditions albeit no significant difference was observed **(Supplemental Figure 2b)**. The lack of difference between the two conditions may largely be due to inconsistencies associated with the TEER chopstick electrode which lead to increased variability compared to the dextran permeability assay. For this reason, TEER was used as a validation tool for confirming barrier stability and not as a means of comparing barrier integrity between conditions. Future iterations of the millifluidic device will incorporate a robust TEER system to allow for live tracking of TEER changes during flow and reduced TEER data variability.

Lastly, validation of the BBB model was performed involving all three cells of the BBB. This was made possible via high magnification (20x, 40x) imaging of immunofluorescent cell-specific markers, specifically PECAM-1, NG2, and GFAP targeting HBMECs, PCs, and ACs, respectively (**Figure 3**). Monolayers of ECs formed on the abluminal membrane of the transwell inserts as determined by confocal microscopy (**Figure 3c,e**). Integrity of the EC monolayer was confirmed by strong PECAM-1 signal localized to cell-cell junctions (**Figure 3e**). On the luminal membrane, NG2 and GFAP fluorescence confirmed the presence of PCs and ACs (**Figure 3b,d,e**) while highlighting astrocyte foot processes extending from the AC cell body throughout the co-culture model (**Figure 3e**). 3D projections of the co-culture (**Figure 3c,d**) convey the multicellular

geometry of the model. A 1:1:1 seeding ratio of HBMECs, PCs, and ACs provided the most stable TEER, substantial PECAM-1 staining, and robust astrocytic foot processes. In terms of physiological relevance of the chosen ratio, this ratio provided optimal BBB properties for our given system and thus the closest approximation to an in vivo environment. Considering that previously published BBB models have suggested ratios ranging from 1:1:1, 1:1:5, and 2:1:1[77-79], our ratio agrees with what has been previously published.

Application of Transwell Millifluidic System to Show that, Under Static Conditions, Adding Astrocytes and Pericytes to Endothelial Cell Monolayers Strengthens BBB Model Barrier Integrity

The contributions of PCs and ACs to barrier integrity of the BBB model were investigated via a dextran permeability assay (**Figure 4a**). Normalizing the permeability coefficients to the average permeability coefficient for the EC monolayer samples, on a per experiment basis, negated the effects of cell passage number to more accurately assess relative differences between conditions.

For the 40 kDa dextran permeability analysis, the individual addition of PCs to HBMECs (denoted as "EP" in Figure 4) as well as ACs to HBMECs (denoted as "EA" in Figure 4) decreased the permeability of the BBB model in comparison with the HBMEC monolayer (denoted as "E" in Figure 4). Specifically, EP samples had a normalized mean permeability coefficient of 0.320 ± 0.0441, a statistically significant ~66% decrease from HBMEC monolayers **(Figure 4b)**. A similar ~66% decrease from HBMEC monolayers was observed in EA samples, which had a normalized mean permeability coefficient of 0.328 ± 0.0538 (**Figure 4b**). We also found that EC/PC/AC co-cultures (denoted as "EPA" in Figure 4) had a normalized permeability coefficient of 0.330 ± 0.100, which was significantly lower (decreased permeability) than what was found for HBMEC monolayers but not statistically different from what was found for EC/AC or EC/PC co-cultures **(Figure 4b)**.

To further investigate barrier integrity of the various cultures, 3 kDa dextran permeability assays (**Figure 4c**) were also performed because, as it is well-established, smaller dextran molecules will enable characterization of BBB permeability at greater resolution[80-82]. With this, small differences in barrier integrity may become more apparent when a smaller molecule permeates through the BBB model. For reference, the raw permeability coefficients for both the 40 kDa and 3 kDa dextran permeability analyses are provided in the table shown in **Figure 4d**. For both 40 kDa and 3 kDa dextran assays, raw permeability coefficients were within range of previous studies conducted[83-86]. However, it should be noted that some studies using FITC conjugated dextran reported slightly lower permeabilities compared to the Texas Red dextran used in this study, likely due to repulsion forces between negative charge on FITC and negative charge on the surface of GCX covered endothelium. The table in **Figure 4d** clearly shows that the BBB is more permeable to 3 kDa dextran than it is to 40 kDa. In addition, in the table in **Figure 4d**, the 3 kDa dextran appears to detect differences in permeability that the 40 kDa dextran cannot resolve. Looking at the normalized data, it is observed that 3 kDa dextran permeability, like 40 kDa dextran permeability, was reduced in the EC/PC, EC/AC and EC/PC/AC co-cultures with normalized permeability values of 0.363 ± 0.0608, 0.683 ± 0.0519, and 0.521 ± 0.0337 respectively **(Figure 4c)**. Interestingly, EC/PC samples exhibited significantly lower permeability than the EC/AC samples and a ~16% decrease in permeability compared to EC/PC/AC samples albeit insignificant **(Figure 4c)**. This data from the 3 kDa dextran permeability assays indicates that both PCs and ACs help improve BBB integrity, but they may act in slight opposition to each other.

Over recent decades, many studies have identified beneficial roles of both PCs and ACs in BBB regulation[17-22]. For example, the addition of PCs and ACs to brain EC monolayers has been shown to reduce permeability to fluorescent dextran[24, 32, 43, 87]. In agreement with these findings, we observed a statistically significant reduction in dextran permeability in the EC/AC, EC/PC, and EC/PC/AC co-cultures compared to HBMEC monolayers, suggesting a beneficial role of both ACs and PCs. However, we did not observe a compounding effect on permeability when both ACs and PCs were cultured with HBMECs, independent of whether permeability was assessed by using the 40 kDa dextran or by using the 3 kDa dextran. For the 40 kDa dextran, this may be due to the fact that the individual addition of either ACs or PCs leads to strong barrier formation in which permeability to relatively large molecules (eg. 40 kDa dextran) has already been sufficiently impeded. The 3 kDa dextran likely clarifies more permeability differences because it is not as limited as 40 kDa by a barrier threshold. Contradictory to the 40 kDa dextran experiment, with the 3 kDa dextran experiment, significant difference in permeability was observed when comparing EC/AC, EC/PC, and EC/PC/AC co-cultures to each other. Compared to HBMEC monolayers, we observed less permeability in the EC/AC condition, followed by less permeability in the EC/PC/AC condition, and followed by the least permeability in the EC/PC condition. This result indicated that pericytes may be playing a stronger role in barrier integrity compared to astrocytes although they both decrease permeability compared to the HBMEC monolayer. For the pericyte co-culture, this observation agrees with previous findings where it was found that pericytes are critical in promoting tight junction protein expression while reducing endothelial transcytosis through the inhibition of molecules which increase vascular permeability[18,88]. Astrocytes on the other hand have a more complex relationship with BBB permeability and may play a dual-role in overall barrier integrity[89]. Astrocytes have been shown to release a variety of factors which ultimately affect the expression of tight junction proteins like ZO-1, claudin-5, and occludin. Astrocyte-derived factors which may increase vascular permeability include VEGF, MMPs, and NO[90-92]. Conversely, several astrocyte-derived factors have demonstrated protective barrier properties like ANG-1 and SHH[93, 94]. These opposing molecular pathways may be the reason why the EC/AC co-culture exhibits greater permeability than the EC/PC condition.

Various studies demonstrate conflicting findings to address the question of whether there should be compounding effects of astrocytes and pericytes on BBB integrity (**Supplemental Figure 2c**)[95]. Although Nakagawa et al. reported increased TEER values for the tri-culture system compared to ACs co-cultured with ECs or PCs co-cultured with ECs, no such increase was observed in the permeability coefficients of sodium fluorescein[96, 97]. Other studies investigating the role of PCs and ACs on BBB integrity also do not report a compounding effect of the two cell types[98, 99]. The beneficial effects of a tri-culture system may not solely be related to decreased permeability but could add physiological relevance in terms of immune response, BBB maintenance, and alternate transport pathways[100]. Regardless, both astrocytes and pericytes decrease permeability compared to the EC monolayer.

Flow Stimulates Improved Barrier Integrity of the HBMEC Monolayer but has Negligible Effects on Integrity of the HBMEC/PC/AC co-culture BBB Model

We also investigated the impact of flow exposure on BBB barrier integrity, using the EC/PC/AC co-culture model. Interestingly, the application of flow for 24 hours at a shear stress of 12 dynes/cm^2 to the EC/PC/AC co-culture BBB model had no impact on dextran permeability using 3 kDa and 40 kDa dextrans (**Figure 5B,C**). A 24-hour flow exposure duration was selected based on previous publications examining the effects of shear stress on BBB integrity[101-103];

supporting the notion that 24 hours provides adequate time to observe permeability changes under flow conditions. When compared to a normalized static control, BBB uniform flow exposure only reduced permeability by 3.26% and 4.36% when using 40 and 3 kDa dextran respectively, with no significance (**Figure 5B,C**). However, because ECs have been shown to benefit from shear stress exposure, the same experiment was performed on HBMEC monolayers. In this case, shear stress exposure successfully reduced permeability to 40 and 3 kDa dextran by a statistically significant 22.3% and 52.5%, respectively, compared to static controls (**Figure 5B,C**).

We postulate that the observed findings in the EC/PC/AC co-culture BBB model may be due to insufficient EC expression of mechanotransducers, which sense and respond to mechanical stimuli. For example, insufficient endothelial glycocalyx (GCX), which is a polysaccharide coat that encapsulates endothelial and other cells, and is a known mechanotransducer, has been shown to regulate EC permeability[104-106]. This implies that perhaps EC GCX expression is low in the EC/PC/AC co-culture BBB model, possibly due to the limited necessity for EC GCX based on the barrier that is provided by the multiple cells and their intercellular junctions. Subsequently, this diminishment in EC GCX expression in the EC/PC/AC co-culture BBB model would disable the ECs' ability to sense and respond to fluid flow and thus their ability to downregulate permeability. Alternatively, the observed results could be due to changes in EC/PC/AC communication when comparing static to flow conditions. For example, the astrocyte-derived factors that may increase permeability, factors such as VEGF, MMPs and NO, may be upregulated in flow conditions. An upregulation of these factors could mitigate the positive effects of flow seen with the EC monolayer alone[64-66].

It should also be noted that the transport study is limited due to dextran transport primarily occurring through paracellular pathways[64]. Transcytosis involvement in dextran transport in our model is most likely limited, as the expression of required membrane transporters that could facilitate dextran transcytosis has not been identified thus far in ECs. Furthermore, dextran transcytosis has been shown to occur at an inconsequentially slower rate than the duration (1 hour) that we employed for our dextan permeability assay[107]. Since our assessment of dextran transport does not explore all transport avenues, it is unreasonable to make final conclusions of the role of the supportive cells and flow on barrier integrity in our BBB model. Future studies will expand the molecular tracers used (e.g., albumin as a transcytosis tracer and/or glucose to measure carrier mediated transport[108, 109]) to fully investigate the implications of astrocytes, pericytes, and flow on various BBB permeability pathways. The device that has been described herein will enable these investigations and further our understanding of BBB regulation in both physiological and pathological conditions.

Western Blot Studies Show Pericytes and Astrocytes, in the Absence and Presence of Flow, Adjust HBMEC ZO-1 and Occludin Expression, and Claudin-5 to Some Extent, to Regulate BBB Permeability

To identify potential molecular mechanisms responsible for the observed changes in BBB permeability as a result of HBMEC co-culture with PCs and/or ACs and/or as a result of flow exposure, protein level analysis via western blotting was performed. In static samples, western blotting identified a statistically significant decrease in occludin expression in HBMECs from EC/PC co-cultures (41.2 ± 3.5% decrease) and EC/PC/AC co-cultures (43.2 ± 7.3% decrease) as compared to HBMEC monolayers (**Figure 6a,b**). In EC/AC co-cultures, a 14.4 ± 9.6% reduction in occludin expression was also observed, but this was not statistically significant. Collectively, this data suggests that the addition of PCs to HBMEC monolayers may actually decrease HBMEC

occludin expression, while the impact of ACs is unclear. In addition to the observed decrease in occludin expression, we also most notably identified changes in claudin-5 expression. Specifically, we identified increased claudin-5 expression in EC/PC, EC/AC, and EC/PC/AC conditions of 53.6 ± 24.6%, 35.3 ± 27.1%, and 42.2 ± 43.1%, respectively (**Figures 6a,b**). While these changes were not statistically significant, the trends suggest that both PCs and ACs may increase the expression of claudin-5 upon co-culture. With regard to ZO-1 expression, we additionally observed a 25 ± 16.8% increase in HBMECs from EC/PC co-cultures when compared to HBMEC monolayers. However, this increase was not statistically significant (**Figures 6a,b**). The expression of VE-cadherin and caveolin-1 was also analyzed, but no changes in either protein were observed. Normalized values for junctional protein expression in co-culture models are provided in **Supplemental Table 2a** while the results from the associated statistical analyses are presented in **Supplemental Table 2b**.

It is complicated to compare protein expression data with previously existing models due to the wide variety of cell types, substrates, and plating methods. However, Nakagawa et al. demonstrated significant increases in claudin-5 and ZO-1 expression levels, with no significant change in occludin expression, for a similar primary tri-culture model compared with just the endothelial monolayer[96]. Thompson et al. observed complicated tight junction differences between culture conditions when examining mRNA levels, finding an upregulation in claudin-5 levels when co-cultured with porcine pericytes but no significant change in tri-culture conditions[99]. Based on these corroborating results, there is no clear expectation of tight junction levels to necessarily increase in tri-culture conditions, but claudin-5 variations seem to be the most indicative of changes in barrier integrity. Future work will attempt to elucidate the importance of individual tight junctions and implicate their roles in BBB maintenance.

The impact of 24-hour 12 dynes/cm^2 shear stress flow exposure on HBMEC tight junction protein expression was also investigated for ZO-1, claudin-5, and occludin. The impact of flow on VE-cadherin and caveolin-1 expression was not investigated as no substantial changes in the expression of these proteins were observed in the static mono- and co-culture BBB models. In EC/PC/AC co-cultures, we found that flow exposure led to a statistically significant increase in HBMEC ZO-1 expression (22.2 ± 5.8% increase) compared to static conditions. In contrast, exposure of HBMEC monolayers to flow led to a negligible 1.9 ± 13.6% increase in ZO-1 expression, which was statistically insignificant (**Figure 6c,d**). Additionally, in both the co-culture and monolayer models, shear stress application resulted in a statistically significant reduction in both claudin-5 and occludin expression. Particularly, occludin expression was reduced by 44.1 ± 5.2% and 54.2 ± 6.3% in EC/PC/AC co-cultures and HBMEC monolayers, respectively, while claudin-5 expression was reduced by 24.7 ± 4.4% and 45.9 ± 9.3%, respectively (**Figure 6c,d**). Normalized values and statistical analysis results for junctional protein expression following flow are provided in **Supplemental Table 3**.

Previous studies implicating PCs and ACs in regulating BBB integrity, specifically BBB permeability, have typically attributed reduced permeability to increased expression of tight junction proteins such as ZO-1, claudin-5, and occludin[19, 24, 32]. The contribution of other proteins to barrier integrity, such as VE-cadherin and caveolin-1, have also been investigated to lesser extents[26, 27]. Here, we found that the addition of both PCs and ACs to HBMECs led to the increased expression of claudin-5 in static conditions, albeit statistically insignificant. When flow conditions were superimposed, while claudin-5 was decreased in flow-conditioned HBMEC monolayers the addition of PCs and ACs reversed the claudin-5 decrease to a negligible extent. We also observed increased ZO-1 expression in EC/PC co-cultures compared to HBMEC monolayers in static

conditions, and this too was statistically insignificant. The role of ZO-1 was made apparent in flow conditions, as we observed that EC/PC/AC co-culture exposure to flow statistically significantly up regulated ZO-1 expression by HBMECs. Taken together, these results suggest that decreased dextran permeability following the addition of PCs and/or ACs to HBMECs relies most heavily on increased ZO-1 and may also depend on increased claudin-5 to a very limited extent. Focusing on occludin, we also observed a statistically significant decrease in occludin expression in both EC/PC and EC/PC/AC co-cultures in static and flow conditions, suggesting that occludin's role is to step down during the observed reduction of BBB permeability. These ZO-1, claudin-5, and occludin results highlight the complex regulation of BBB permeability. Beyond these three proteins, BBB permeability depends on the expression and function of dozens of other proteins. Thus, PCs and ACs may also induce HBMECs to regulate BBB permeability through alternative EC proteins and structures not investigated in this study. These may include ABC transporters, such as P-glycoprotein, integrins, or junctional adhesion molecule, such as JAM-A, all of which have been implicated in regulating BBB permeability [110-112]. Future studies should investigate these and other alternative mechanisms of HBMEC and BBB regulation by PCs, ACs, and flow.

Immunocytochemical Studies Reveal that Pericytes and Astrocytes, as well as Flow Conditions, Support ZO-1/Claudin-5 Expressing Junction Development and Robust Glycocalyx Formation

To further interrogate the potential molecular mechanisms responsible for BBB permeability adaptations due to HBMEC co-culture with PCs and/or ACs and due to incubation of the cells in the absence versus presence of perfusing fluid, fluorescence ICC was implemented as an additional approach to performing protein level analysis. First, we identified the junctional localization of ZO-1 and claudin-5. Occludin was not stained for in conjunction with ZO-1 and claudin-5 due to the observations made with the Western blot studies, in which we found down regulation of occludin in correlation to increasing permeability due to co-culture in static conditions, and under flow conditions. ZO-1/claudin-5 co-staining in HBMEC monolayers as well as EC/PC, EC/AC, and EC/PC/AC co-cultures demonstrated substantial junctional localization of both proteins as anticipated (**Figure 7a**). In static conditions, HBMEC monolayers, EC/PC co-cultures, and EC/PC/AC co-cultures demonstrated the strongest claudin-5 staining, and in EC/AC co-cultures claudin-5 expression seemed diminished. However, expression and junctional localization of ZO-1 in these samples remained consistent. Similar to what was observed with western blotting data, co-staining of flow-exposed HBMEC monolayers and EC/PC/AC co-cultures demonstrated a significant reduction in claudin-5 expression, when compared to static conditions (**Figure 7a**). An increase in ZO-1 expression and localization at cell-cell junctions in flow-exposed HBMEC monolayers and EC/PC/AC co-cultures was also observed. Taken together, ICC of these tight junction proteins suggests that BBB permeability may not solely be affected by the protein expression level but may also be altered by distribution and localization. Furthermore, tight junction proteins like ZO-1 may prove to be more influential on overall BBB permeability than claudin-5 based on the correlations between the dextran permeability, western blot, and ICC data.

From ZO-1 and claudin-5 co-stained fluorescent micrographs we made another observation worth noting, pertaining to the question about the ability of brain ECs to align with flow. We observed that the ZO-1/claudin-5-stained HBMECs in the flow conditioned EC/PC/AC co-culture, compared to other conditions (e.g., monoculture or static), appeared to exhibit the most prominent HBMEC alignment in the direction parallel to the flow stream (**Figure 7a**). This observation is of

great interest, considering the limited prior reports of HBMECs in monoculture aligning in the direction of flow[66-68] and recalling our own observations of HBMEC alignment primarily at low seeding densities (**Supplemental Figure 3**). Although this observation is purely qualitative, it seems to indicate that supportive cells as well as flow conditions are necessary for HBMEC alignment in vitro.

Circling back to the BBB permeability discussion, in search of other potential molecular mechanisms recall that BBB permeability is not only controlled by the tight junctions as has been our focus, or by the transporters or junctional adhesion molecules that we mentioned above. We have already speculated that there is possible involvement of the EC GCX in the BBB permeability detected in our system. For example, we suggested that in the EC/PC/AC co-culture there may be insufficient EC GCX to convert the flow stimulus into decreased permeability. This suggestion is supported by prior published proposals that BBB permeability can be mediated by the mechanosensitive and EC monolayer protective GCX [113-115]. There is also prior published demonstration that GCX regulates cerebral vascular permeability through restricting molecular adhesion to the endothelium as well as acting as a charge barrier due to its high degree of net negative charge[66-68]. Although the GCX is believed to play a role in regulating BBB permeability, its function is still understudied and poorly understood. We hope to utilize our new millifluidic transwell system to begin to generate new knowledge about the HBMEC GCX in the BBB.

As a starting point, in the present study the HBMEC GCX was fluorescently labeled in monoculture, co-culture, static, and flow environments. Specifically, the HBMEC GCX was labelled with wheat germ agglutin (WGA) lectin **(Figure 7b)**. WGA is a preferred stain for broadly labelling the GCX due to its ability to bind to multiple GCX components including sialic acid, the n-acetylglucosamine component of hyaluronic acid, and the n-acetylglucosamine component of heparan sulfate[116]. Based on WGA imaging, GCX expression appears to be drastically reduced in static EC/AC conditions compared with HBMEC monolayer, EC/PC, and EC/PC/AC conditions. EC/PC/AC static conditions seemed to have the highest WGA fluorescent intensity overall. As expected from previous studies[62, 116], the introduction of flow to the HBMEC monolayer increased GCX abundance compared to static conditions. Yet, interestingly, when EC/PC/AC co-cultures were exposed to flow, compared to their static counterparts, there was no increase in WGA fluorescence. Perhaps the tri-culture condition limits the cellular response to flow due to an already substantial GCX which would correlate with the observed trend in no significant change in permeability between flow and static conditions in the tri-culture. The results collectively indicate that either the introduction of astrocytes and pericytes or the application of shear stress may support increased GCX development, but co-culture and flow don't necessarily need to be simultaneously applied to develop the GCX, due to a potential GCX threshold. Furthermore, the results point to the importance of incorporating supportive cells and flow conditions in experimental in vitro models of the BBB, for improved GCX growth which is a key feature in the pursuit of a physiologically relevant system. Lastly, to reiterate, our purpose of examining GCX expression was to further investigate potential mechanisms for the observed changes in BBB permeability in different conditions. Although tight junctional proteins are often implicated in primarily regulating the permeability of the BBB, clearly there is potential for the GCX to have a role as well. Further studies will aim to utilize the transwell microfluidic device to explore the relationship between BBB permeability, tight junction expression, and GCX in flow and co-culture conditions.

CONCLUSION

This study describes a novel millifluidic device that is both easy to utilize and compatible with numerous upstream and downstream experimental tasks, as summarized below.

First, cell seeding and culturing can be problematic in common (e.g., PDMS) microfluidic devices. In contrast, the compatibility of our device with transwell inserts allows for easy cell seeding and culturing including co-culturing of multiple cell types. Second, common microfluidics fabricated out of PDMS are often limited by issues with microbubble formation. The fabricated transwell millifluidic device avoids microbubble formation via the use of larger channel dimensions. Third, common microfluidic devices can also have limited compatibility with downstream analytical techniques[50] such as high magnification microscopy and western blotting, but the fabricated transwell millifluidic circumvents these issues using a design compatible with disassembly. Fourth, like microfluidic devices our millifluidic system has the potential for higher throughput. We are currently developing the next iteration of the device to accommodate multiple transwell inserts in series and in parallel to expand throughput. Therefore, as our millifluidic device requires minimal knowledge about the design, is easy to use compared to a microfluidic system, and has high throughput potential, it is a more feasible option for individuals without microfluidic expertise who are interested in investigating shear stress effects on the BBB. Additionally, in contrast with many previous BBB models that utilized non-human or immortalized cell lines and therefore lack physiological relevance[47-49, 58-61], our model contains only primary human cells, which provides increased confidence of results and conclusions that are relevant to human physiology and disease.

We were able to confirm that the millifluidic device induces EC alignment. In addition to the observed impacts of flow on cell alignment, we also found that flow exposure reduced dextran permeability in HBMEC monolayers. Furthermore, using a transwell BBB model (consisting of HBMECs, human ACs, and human PCs) embedded in the novel millifluidic device, a beneficial role of both ACs and PCs on BBB integrity was identified. These results can be further examined in the future, particularly to investigate (1) the EC mechanotransducers responsible for the observed impact of flow exposure on BBB integrity and (2) the specific mechanisms through which astrocytes and/or pericytes support ECs to improve BBB barrier integrity. Regarding mechanisms, although this study was only intended to validate our novel millifluidic device, it provided some clues regarding the complex cellular pathways involved in the BBB response to flow exposure. Specifically, while tight junction protein production was upregulated when ACs and PCs were introduced to the HBMECs, no such response was apparent under flow conditions. However, shear stress seems to increase ZO-1 localization expression at cellular junctions. Additionally, GCX expression may be more robust in tri-culture or flow conditions. These results should be interrogated in future studies. Ideally, such studies will lead to the identification of unique therapeutic targets for restoring BBB function in numerous neurological pathologies.

AUTHOR CONTRIBUTIONS

I.C.H., I.M.H., and E.E.E. developed and designed the study. I.C.H., N.R.O., I.M.H., and E.E.E. provided insight on study results. I.C.H., N.R.O., M.V., A.C., C.I.L., and K.M. conducted experiments. I.C.H., N.R.O., M.V., K.M., I.M.H., and E.E.E. wrote and revised the manuscript.

CONFLICTS OF INTEREST

The authors declare that U.S. Patent Application (No. 17/454,768) has been filed for Hanging Cell Culture Millifluidic Device.

FIGURE & TABLE CAPTIONS

Figure 1: *Blood brain barrier millifluidic device.* (A) Schematic of the blood-brain barrier in vivo. (B) Expanded view of the blood-brain barrier transwell millifluidic device. (C,D) Outline of the transwell plating protocol for both (C) flow experiments and (D) experiments performed in static conditions. (E) Views of the computational model demonstrate that the HBMECs directly contact fully developed flow patterns and shear stress levels that are at 12 dynes/cm^2, comparable to flow experienced by ECs in vivo. In the view on the right, the concentric circles on the center of the image indicate the location of the transwell insert. (F) Live tracking of fluorescent microspheres validated the expected flow patterns predicted by the computational model. (G) Schematic of the TEER protocol used to analyze HBMEC monolayer integrity. (H) HBMEC TEER values in static conditions over a five-day period demonstrate peaked barrier integrity following the third day of culture.

Figure 2: *Human Brain endothelial cells (HBMECs) do not align in the direction of flow while Human Aortic Endothelial Cells (HAECs) align parallel to flow.* (A) Representative images are shown of HBMEC cells after 24 hours of flow exposure at 12 dynes/cm^2. HBMECs do not readily align in the flow direction and may align perpendicular to flow when cultured on the transwell in a monolayer. (B) HAEC cell alignment in the direction of flow after 24 hours of flow exposure at 12 dynes/cm^2 in the Transwell Millifluidic device demonstrates parallel alignment.

Figure 3: *Validation of Transwell BBB model. En face* fluorescent images showing the (A) human brain microvascular endothelial cells and (B) the human brain pericytes and astrocytes within the co-culture BBB model. Three-dimensional perspective of the transwell BBB co-culture via the (C) endothelial cell side and (D) the pericyte-astrocyte side. (E) Higher magnification imaging demonstrates (top) strong junctional PECAM-1 signal (white arrows) in HBMECs, (bottom left) GFAP expression with identifiable processes in astrocytes (dashed yellow lines), and (bottom right) NG2 expression in pericytes.

Figure 4: *Dextran permeability analysis identifies astrocyte and pericyte roles in lowering BBB.* (A) Schematic of the dextran permeability assay in static-conditioned cultures. (B) In comparison to HBMEC monolayers (E), 40 kDa dextran permeability analysis demonstrates a decrease in permeability in EC/PC (EP), EC/AC (EA) and EC/PC/AC (EPA) co-cultures when normalized to the average value of the HBMEC monolayer (E). (C) While the 3 kDa dextran permeability analysis still exhibits a decrease in permeability of the three cultures compared to the HBMEC monolayer (E), there is also a significant increase in permeability of the EA culture compared to EP and EPA and a significant decrease in permeability of the EP culture compared to EA and EPA. (D) Permeability coefficients (cm/s) of 40 kDa and 3 kDa dextran for E, EP, EA, and EPA cultures. Data corresponds to Figures 4b and 4c. (For Figures 4b and 4c, * denotes $p<0.05$; ** denotes $p<0.01$; and *** denotes $p<0.001$.)

Figure 5: *Dextran permeability shows that flow exposure improves barrier integrity in HBMEC monolayers but not co-culture BBB models.* (A) Schematic of the dextran permeability assay in flow-conditioned cultures with opposite cellular orientation. (B) 40 kDa dextran permeability analysis demonstrates a statistically significant decrease in permeability in E flow conditions vs

static but no apparent difference in EC/PC/AC (EPA) co-cultures. Raw permeability values were normalized to static controls to account for differences in cell passage number and other experimental factors. (C) Similarly, 3 kDa dextran permeability analysis demonstrated the same trend of a significant reduction in BBB permeability in E flow conditions vs. static conditions. (D) Permeability coefficients (cm/s) of 40 kDa and 3 kDa dextran for E static, E flow, EPA static, EPA flow conditions. Data corresponds to Figures 5b and 5c. (For figure 5b and 5c, * denotes $p<0.05$)

Figure 6: *HBMEC (E) occludin appears to be the most statistically significantly regulated protein in static conditions, particularly due to co-culture of the HBMECs with pericytes. HBMEC (E) ZO-1, claudin-5, and occludin are all statistically significantly regulated in flow conditions when HBMECs (E) are co-cultured with both ACs and PCs (to form the EC/PC/AC (EPA) BBB model).* (A) Western blot quantification of HBMEC ZO-1, occludin, claudin-5, VE-cadherin, and caveolin-1 expression in HBMEC monolayers (E), EC/PC (EP) co-cultures, EC/AC (EA) co-cultures, and EC/PC/AC (EPA) co-cultures. Occludin expression is significantly reduced in both EC/PC (EP) and EC/PC/AC (EPA) conditions. (B) Representative western blot bands. (C) Western blot quantification of HBMEC ZO-1, occludin, and claudin-5 in both EC/PC/AC (EPA) co-cultures and HBMEC monolayers (E) after flow exposure. Dotted line represents static condition values by which the experimental data is normalized. Flow exposure increases ZO-1 expression in the tri-culture model but reduces claudin-5 and occludin in both the tri-culture and HBMEC monolayer models. (D) Representative western blot bands. (For Figures 6a and 6c, * denotes $p<0.05$; ** denotes $p<0.01$; *** denotes $p<0.001$; and **** denotes $p<0.0001$.)

Figure 7: *Immunocytochemistry (ICC) of ZO-1, claudin-5, and WGA demonstrate strong junctional localization and varying GCX expression; cell orientation with respect to flow direction is also clarified.* (A) ZO-1 and claudin-5 immunocytochemistry in HBMEC monolayers and EC/PC, EC/AC, and EC/PC/AC co-cultures in static and flow conditions. Strong junctional signal can be seen in all samples. ICC of HBMEC monolayers and EC/PC/AC co-cultures exposed to flow highlight reduced claudin-5 expression and increased ZO-1 junctional thickness following flow. It can also be observed that the ZO-1/claudin-5-stained HBMECs in the flow conditioned EC/PC/AC co-culture exhibit the most prominent alignment with the direction of flow, when compared to other conditions (e.g., monoculture or static). (B) WGA staining of EC, EC/PC, EC/AC, and EC/PC/AC in static and flow conditions demonstrates varying GCX abundance in the different conditions. Tri-culture and/or flow conditions reveal increased WGA fluorescent intensity and GCX thickness.
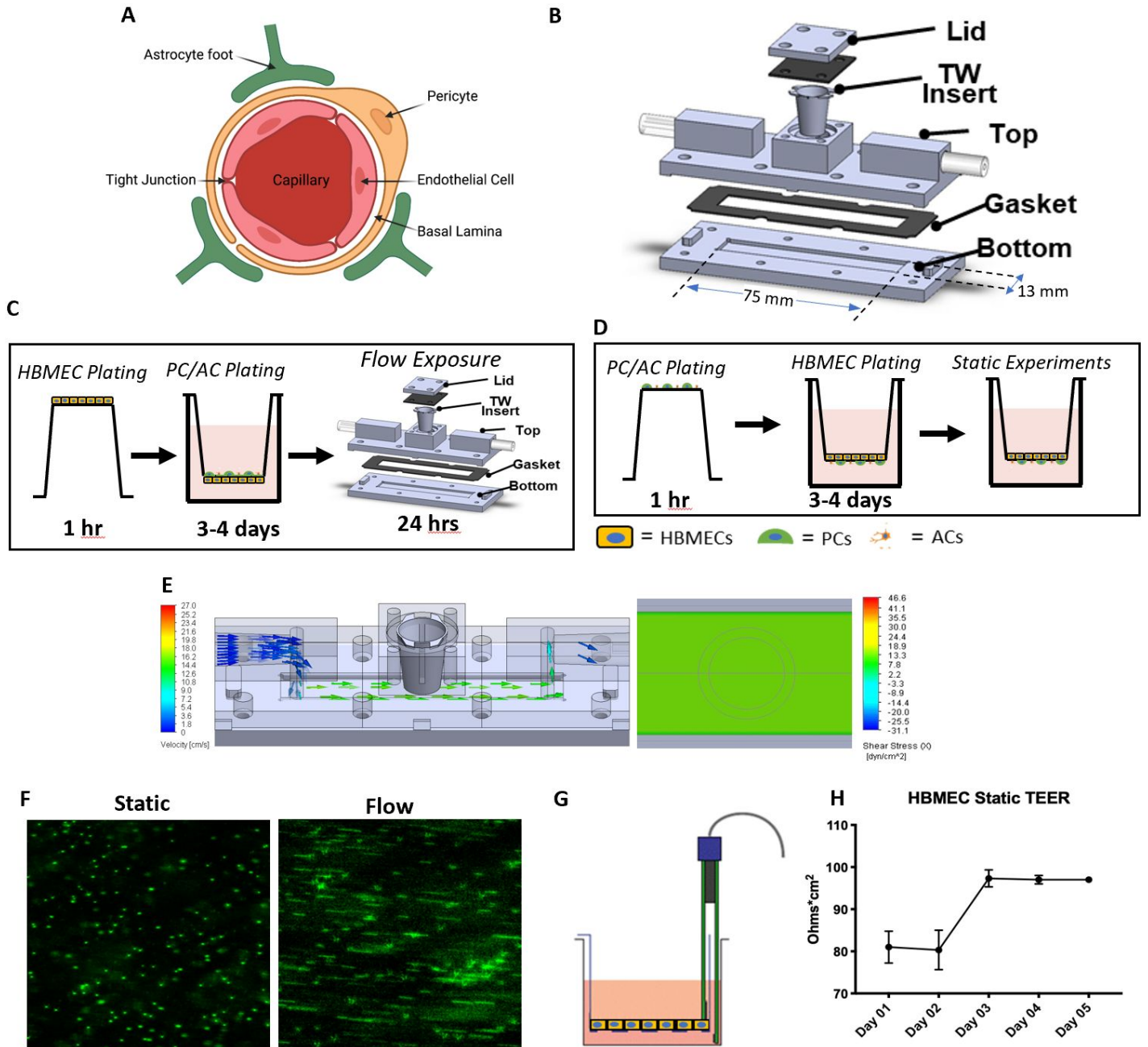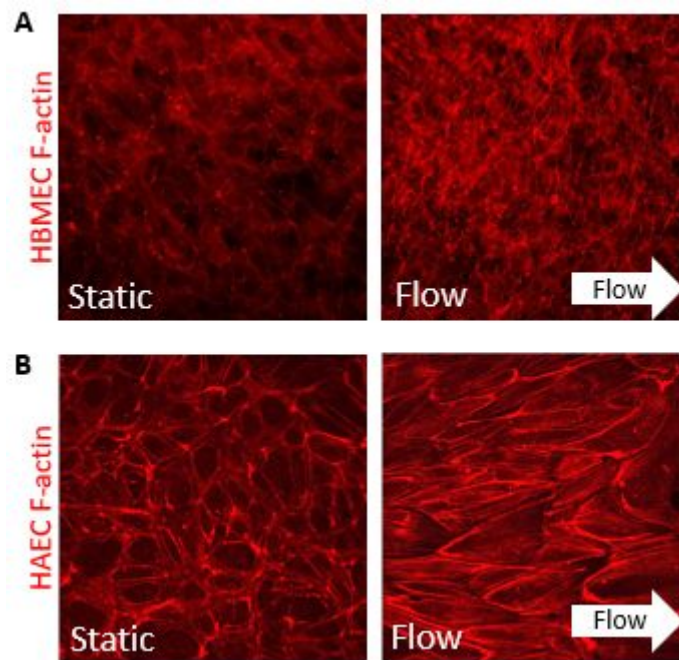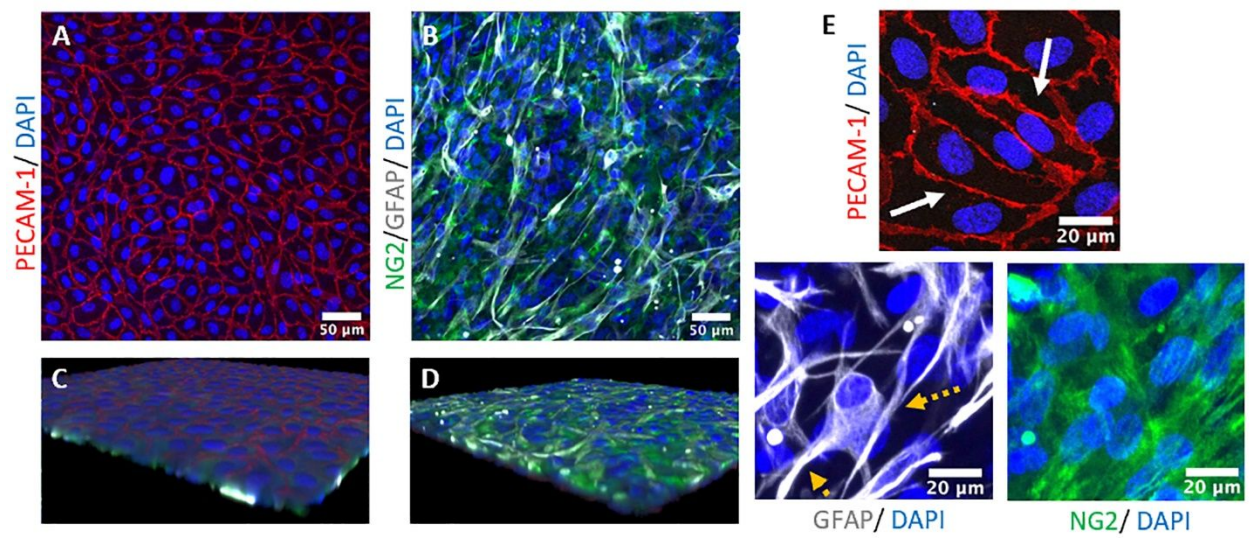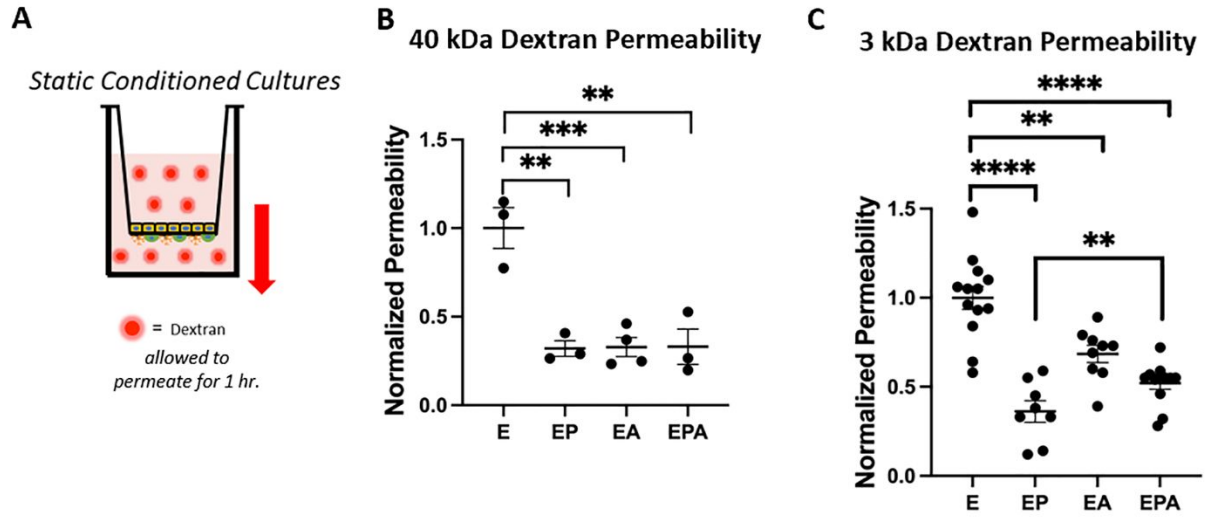
22

Figure 1

Figure 2

Figure 3

Figure 4

A

Static Conditioned Cultures

⬤ = Dextran
*allowed to
permeate for 1 hr.*

B

40 kDa Dextran Permeability

** , *** , **

C

3 kDa Dextran Permeability

**** , ** , **** , ****

D **Permeability Coefficients**

	E	EP	EA	EPA
40 kDa	$6.77 \times 10^{-7} \pm 7.80 \times 10^{-8}$	$2.17 \times 10^{-7} \pm 3.01 \times 10^{-8}$	$2.22 \times 10^{-7} \pm 3.64 \times 10^{-8}$	$2.67 \times 10^{-7} \pm 6.47 \times 10^{-8}$
3 kDa	$1.85 \times 10^{-5} \pm 1.04 \times 10^{-6}$	$7.76 \times 10^{-6} \pm 1.06 \times 10^{-6}$	$1.49 \times 10^{-5} \pm 1.05 \times 10^{-6}$	$9.69 \times 10^{-6} \pm 7.48 \times 10^{-7}$

Lab on a Chip

Figure 5

A

Flow Conditioned Cultures

● = Dextran

*allowed to
permeate for 1 hr.*

B 40 kDa Dextran Permeability

C 3 kDa Dextran Permeability
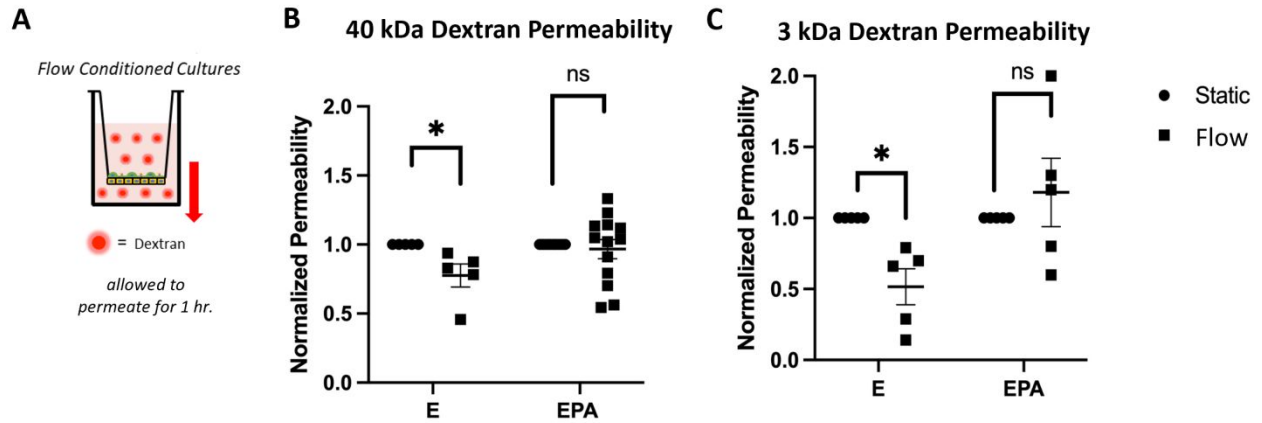
● Static
■ Flow

D Permeability Coefficients

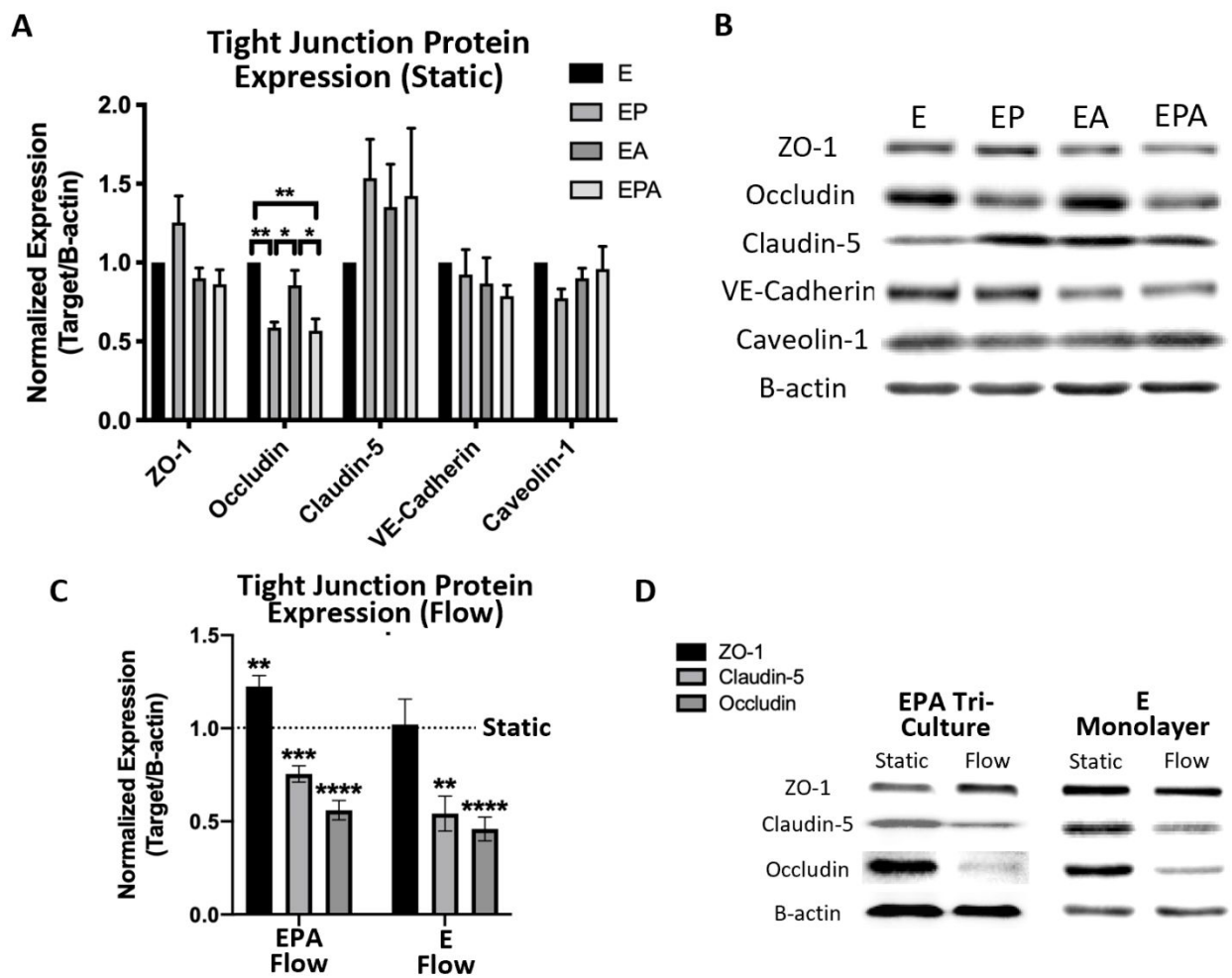|	E Static	E Flow	EPA Static	EPA Flow
40 kDa	$4.06 \times 10^{-7} \pm 7.61 \times 10^{-8}$	$3.21 \times 10^{-7} \pm 6.94 \times 10^{-8}$	$1.88 \times 10^{-7} \pm 3.53 \times 10^{-8}$	$1.81 \times 10^{-7} \pm 4.01 \times 10^{-8}$
3 kDa	$3.08 \times 10^{-5} \pm 7.61 \times 10^{-6}$	$1.46 \times 10^{-5} \pm 4.51 \times 10^{-6}$	$4.94 \times 10^{-6} \pm 1.49 \times 10^{-6}$	$4.72 \times 10^{-6} \pm 1.19 \times 10^{-6}$

Figure 6

Figure 7

REFERENCES

1. G. B. D. N. Collaborators, *Lancet Neurol*, 2019, **18**, 459-480.
2. M. A. Bell and M. J. Ball, *Acta Neuropathol*, 1981, **53**, 299-318.
3. M. Ujiie, D. L. Dickstein, D. A. Carlow and W. A. Jefferies, *Microcirculation*, 2003, **10**, 463-470.
4. G. L. Bowman, J. A. Kaye, M. Moore, D. Waichunas, N. E. Carlson and J. F. Quinn, *Neurology*, 2007, **68**, 1809-1814.
5. D. M. E. van Assema, M. Lubberink, P. Rizzu, J. C. van Swieten, R. C. Schuit, J. Eriksson, P. Scheltens, M. Koepp, A. A. Lammertsma and B. N. M. van Berckel, *Ejnmmi Res*, 2012, **2**.
6. L. L. Latour, D. W. Kang, M. A. Ezzeddine, J. A. Chalela and S. Warach, *Ann Neurol*, 2004, **56**, 468-477.
7. T. Kahles, P. Luedike, M. Endres, H. J. Galla, H. Steinmetz, R. Busse, T. Neumann-Haefelin and R. P. Brandes, *Stroke*, 2007, **38**, 3000-3006.
8. D. Knowland, A. Arac, K. J. Sekiguchi, M. Hsu, S. E. Lutz, J. Perrino, G. K. Steinberg, B. A. Barres, A. Nimmerjahn and D. Agalliu, *Neuron*, 2014, **82**, 603-617.
9. A. G. Kermode, A. J. Thompson, P. Tofts, D. G. MacManus, B. E. Kendall, D. P. Kingsley, I. F. Moseley, P. Rudge and W. I. McDonald, *Brain*, 1990, **113 (Pt 5)**, 1477-1489.
10. D. Gay and M. Esiri, *Brain*, 1991, **114 (Pt 1B)**, 557-572.
11. S. P. Cramer, H. Simonsen, J. L. Frederiksen, E. Rostrup and H. B. Larsson, *Neuroimage Clin*, 2014, **4**, 182-189.
12. M. K. Baskaya, A. M. Rao, A. Dogan, D. Donaldson and R. J. Dempsey, *Neurosci Lett*, 1997, **226**, 33-36.
13. R. D. Readnower, M. Chavko, S. Adeeb, M. D. Conroy, J. R. Pauly, R. M. McCarron and P. G. Sullivan, *J Neurosci Res*, 2010, **88**, 3530-3539.
14. T. Higashida, C. W. Kreipke, J. A. Rafols, C. Peng, S. Schafer, P. Schafer, J. Y. Ding, D. Dornbos, 3rd, X. Li, M. Guthikonda, N. F. Rossi and Y. Ding, *J Neurosurg*, 2011, **114**, 92-101.
15. N. J. Abbott, A. A. K. Patabendige, D. E. M. Dolman, S. R. Yusof and D. J. Begley, *Neurobiol Dis*, 2010, **37**, 13-25.
16. Y. Persidsky, S. H. Ramirez, J. Haorah and G. D. Kanmogne, *J Neuroimmune Pharm*, 2006, **1**, 223-236.
17. A. Al Ahmad, C. B. Taboada, M. Gassmann and O. O. Ogunshola, *J Cerebr Blood F Met*, 2011, **31**, 693-705.
18. A. Armulik, G. Genove, M. Mae, M. H. Nisancioglu, E. Wallgard, C. Niaudet, L. Q. He, J. Norlin, P. Lindblom, K. Strittmatter, B. R. Johansson and C. Betsholtz, *Nature*, 2010, **468**, 557-U231.
19. R. D. Bell, E. A. Winkler, A. P. Sagare, I. Singh, B. LaRue, R. Deane and B. V. Zlokovic, *Neuron*, 2010, **68**, 409-427.
20. R. Daneman, L. Zhou, A. A. Kebede and B. A. Barres, *Nature*, 2010, **468**, 562-U238.
21. P. J. Gaillard, I. C. J. van der Sandt, L. H. Voorwinden, D. Vu, J. L. Nielsen, A. G. de Boer and D. D. Breimer, *Pharmaceut Res*, 2000, **17**, 1198-1205.
22. Y. Hayashi, M. Nomura, S. I. Yamagishi, S. I. Harada, J. Yamashita and H. Yamamoto, *Glia*, 1997, **19**, 13-26.

23.   S. Nakagawa, M. A. Deli, S. Nakao, M. Honda, K. Hayashi, R. Nakaoke, Y. Kataoka and M. Niwa, *Cell Mol Neurobiol*, 2007, **27**, 687-694.

24.   M. Campisi, Y. Shin, T. Osaki, C. Hajal, V. Chiono and R. D. Kamm, *Biomaterials*, 2018, **180**, 117-129.

25.   T. W. Gardner, E. Lieth, S. A. Khin, A. J. Barber, D. J. Bonsall, T. Lesher, K. Rice and W. A. Brennan, Jr., *Invest Ophthalmol Vis Sci*, 1997, **38**, 2423-2427.

26.   Q. Rui, H. B. Ni, X. L. Lin, X. J. Zhu, D. Li, H. X. Liu and G. Chen, *Exp Neurol*, 2019, **322**.

27.   L. Delsing, P. Donnes, J. Sanchez, M. Clausen, D. Voulgaris, A. Falk, A. Herland, G. Brolen, H. Zetterberg, R. Hicks and J. Synnergren, *Stem Cells*, 2018, **36**, 1816-1827.

28.   Y. Bai, X. Zhu, J. Chao, Y. Zhang, C. Qian, P. Li, D. Liu, B. Han, L. Zhao, J. Zhang, S. Buch, G. Teng, G. Hu and H. Yao, *PLoS One*, 2015, **10**, e0124362.

29.   A. T. Argaw, L. Asp, J. Zhang, K. Navrazhina, T. Pham, J. N. Mariani, S. Mahase, D. J. Dutta, J. Seto, E. G. Kramer, N. Ferrara, M. V. Sofroniew and G. R. John, *J Clin Invest*, 2012, **122**, 2454-2468.

30.   G. Thanabalasundaram, C. Pieper, M. Lischper and H. J. Galla, *Brain Res*, 2010, **1347**, 1-10.

31.   G. Thanabalasundaram, J. Schneidewind, C. Pieper and H. J. Galla, *Int J Biochem Cell Biol*, 2011, **43**, 1284-1293.

32.   V. Siddharthan, Y. V. Kim, S. Liu and K. S. Kim, *Brain Research*, 2007, **1147**, 39-50.

33.   L. Cucullo, M. Hossain, V. Puvenna, N. Marchi and D. Janigro, *Bmc Neurosci*, 2011, **12**.

34.   O. C. Colgan, G. Ferguson, N. T. Collins, R. P. Murphy, G. Meade, P. A. Cahill and P. M. Cummins, *Am J Physiol Heart Circ Physiol*, 2007, **292**, H3190-3197.

35.   T. G. Walsh, R. P. Murphy, P. Fitzpatrick, K. D. Rochfort, A. F. Guinan, A. Murphy and P. M. Cummins, *J Cell Physiol*, 2011, **226**, 3053-3063.

36.   F. Garcia-Polite, J. Martorell, P. Del Rey-Puech, P. Melgar-Lesmes, C. C. O'Brien, J. Roquer, A. Ois, A. Principe, E. R. Edelman and M. Balcells, *J Cereb Blood Flow Metab*, 2017, **37**, 2614-2625.

37.   A. Reinitz, J. DeStefano, M. Ye, A. D. Wong and P. C. Searson, *Microvasc Res*, 2015, **99**, 8-18.

38.   J. G. DeStefano, Z. S. Xu, A. J. Williams, N. Yimam and P. C. Searson, *Fluids Barriers CNS*, 2017, **14**, 20.

39.   Y. He, Y. Yao, S. E. Tsirka and Y. Cao, *Stroke*, 2014, **45**, 2514-2526.

40.   S. Veszelka, A. Toth, F. R. Walter, A. E. Toth, I. Grof, M. Meszaros, A. Bocsik, E. Hellinger, M. Vastag, G. Rakhely and M. A. Deli, *Front Mol Neurosci*, 2018, **11**, 166.

41.   D. E. Eigenmann, G. Xue, K. S. Kim, A. V. Moses, M. Hamburger and M. Oufir, *Fluids and Barriers of the CNS*, 2013, **10**, 33.

42.   K. Hatherell, P. O. Couraud, I. A. Romero, B. Weksler and G. J. Pilkington, *J Neurosci Meth*, 2011, **199**, 223-229.

43.   P. J. Gaillard, L. H. Voorwinden, J. L. Nielsen, A. Ivanov, R. Atsumi, H. Engman, C. Ringbom, A. G. de Boer and D. D. Breimer, *Eur J Pharm Sci*, 2001, **12**, 215-222.

44.   M. Boveri, V. Berezowski, A. Price, S. Slupek, A. M. Lenfant, C. Benaud, T. Hartung, R. Cecchelli, P. Prieto and M. P. Dehouck, *Glia*, 2005, **51**, 187-198.

45.   K. L. Audus and R. T. Borchardt, *Ann N Y Acad Sci*, 1987, **507**, 9-18.

46.   J. B. van Bree, A. G. de Boer, M. Danhof, L. A. Ginsel and D. D. Breimer, *J Pharmacol Exp Ther*, 1988, **247**, 1233-1239.

47.   R. Booth and H. Kim, *Lab Chip*, 2012, **12**, 1784-1792.
48.   B. Prabhakarpandian, M. C. Shen, J. B. Nichols, I. R. Mills, M. Sidoryk-Wegrzynowicz, M. Aschner and K. Pant, *Lab Chip*, 2013, **13**, 1093-1101.
49.   L. M. Griep, F. Wolbers, B. de Wagenaar, P. M. ter Braak, B. B. Weksler, I. A. Romero, P. O. Couraud, I. Vermes, A. D. van der Meer and A. van den Berg, *Biomed Microdevices*, 2013, **15**, 145-150.
50.   M. W. van der Helm, A. D. van der Meer, J. C. T. Eijkel, A. van den Berg and L. I. Segerink, *Tissue Barriers*, 2016, **4**.
51.   A. L. Paguirigan and D. J. Beebe, *Integr Biol (Camb)*, 2009, **1**, 182-195.
52.   B. J. van Meer, H. de Vries, K. S. A. Firth, J. van Weerd, L. G. J. Tertoolen, H. B. J. Karperien, P. Jonkheijm, C. Denning, I. J. AP and C. L. Mummery, *Biochem Biophys Res Commun*, 2017, **482**, 323-328.
53.   S. Halldorsson, E. Lucumi, R. Gomez-Sjoberg and R. M. T. Fleming, *Biosens Bioelectron*, 2015, **63**, 218-231.
54.   S.-H. Chang, P.-L. Ko, W.-H. Liao, C.-C. Peng and Y.-C. Tung, *Micromachines*, 2021, **12**, 406.
55.   S. Hinkel, K. Mattern, A. Dietzel, S. Reichl and C. C. Muller-Goymann, *Int J Pharm*, 2019, **566**, 434-444.
56.   K. Mattern, N. Beissner, S. Reichl and A. Dietzel, *Eur J Pharm Biopharm*, 2018, **126**, 159-165.
57.   E. Mairey, A. Genovesio, E. Donnadieu, C. Bernard, F. Jaubert, E. Pinard, J. Seylaz, J. C. Olivo-Marin, X. Nassif and G. Dumenil, *J Exp Med*, 2006, **203**, 1939-1950.
58.   A. K. Achyuta, A. J. Conway, R. B. Crouse, E. C. Bannister, R. N. Lee, C. P. Katnik, A. A. Behensky, J. Cuevas and S. S. Sundaram, *Lab Chip*, 2013, **13**, 542-553.
59.   H. Cho, J. H. Seo, K. H. Wong, Y. Terasaki, J. Park, K. Bong, K. Arai, E. H. Lo and D. Irimia, *Sci Rep*, 2015, **5**, 15222.
60.   S. P. Deosarkar, B. Prabhakarpandian, B. Wang, J. B. Sheffield, B. Krynska and M. F. Kiani, *PLoS One*, 2015, **10**, e0142725.
61.   K. L. Sellgren, B. T. Hawkins and S. Grego, *Biomicrofluidics*, 2015, **9**, 061102.
62.   I. C. Harding, R. Mitra, S. A. Mensah, I. M. Herman and E. E. Ebong, *J Transl Med*, 2018, **16**.
63.   A. Nicolas, F. Schavemaker, K. Kosim, D. Kurek, M. Haarmans, M. Bulst, K. Lee, S. Wegner, T. Hankemeier, J. Joore, K. Domansky, H. L. Lanz, P. Vulto and S. J. Trietsch, *Lab Chip*, 2021, **21**, 1676-1685.
64.   T. S. Frost, L. Jiang, R. M. Lynch and Y. Zohar, *Micromachines*, 2019, **10**, 533.
65.   J. A. Brown, S. L. Faley, Y. Shi, K. M. Hillgren, G. A. Sawada, T. K. Baker, J. P. Wikswo and E. S. Lippmann, *Fluids and Barriers of the CNS*, 2020, **17**.
66.   P. M. Washington, C. Lee, M. K. R. Dwyer, E. E. Konofagou, S. G. Kernie and B. Morrison, 3rd, *J Cereb Blood Flow Metab*, 2020, **40**, 2026-2037.
67.   H. Kolarova, J. Vitecek, A. Cerna, M. Cernik, J. Pribyl, P. Skladal, D. Potesil, I. Ihnatova, Z. Zdrahal, A. Hampl, A. Klinke and L. Kubala, *Free Radic Biol Med*, 2021, **162**, 14-26.
68.   F. E. Curry and R. H. Adamson, *Ann Biomed Eng*, 2012, **40**, 828-839.
69.   A. Reinitz, J. DeStefano, M. Ye, A. D. Wong and P. C. Searson, *Microvascular research*, 2015, **99**, 8-18.

70.   J. G. DeStefano, Z. S. Xu, A. J. Williams, N. Yimam and P. C. Searson, *Fluids and Barriers of the CNS*, 2017, **14**, 1-15.

71.   M. Ye, H. M. Sanchez, M. Hultz, Z. Yang, M. Bogorad, A. D. Wong and P. C. Searson, *Sci Rep*, 2014, **4**, 4681.

72.   S. N. Rampersad, S. I. Freitag, F. Hubert, P. Brzezinska, N. Butler, M. B. Umana, A. R. Wudwud and D. H. Maurice, *Cell Signal*, 2016, **28**, 606-619.

73.   K. A. Bailey, F. G. Haj, S. I. Simon and A. G. Passerini, *Sci Rep*, 2017, **7**, 8196.

74.   C. A. Dessalles, C. Leclech, A. Castagnino and A. I. Barakat, *Communications Biology*, 2021, **4**.

75.   T. Hara, S. Yabushita, C. Yamamoto and T. Kaji, *International Journal of Molecular Sciences*, 2020, **21**, 3698.

76.   A. C. Vion, T. Perovic, C. Petit, I. Hollfinger, E. Bartels-Klein, E. Frampton, E. Gordon, L. Claesson-Welsh and H. Gerhardt, *Front Physiol*, 2020, **11**, 623769.

77.   G. T. Knipp and K. E. Lubin, *Pharmacy & Pharmacology International Journal*, 2021, **9**, 143-158.

78.   A. Herland, A. D. Van Der Meer, E. A. Fitzgerald, T.-E. Park, J. J. F. Sleeboom and D. E. Ingber, *PLOS ONE*, 2016, **11**, e0150360.

79.   N. L. Stone, T. J. England and S. E. O'Sullivan, *Front Cell Neurosci*, 2019, **13**, 230.

80.   K. Haruwaka, A. Ikegami, Y. Tachibana, N. Ohno, H. Konishi, A. Hashimoto, M. Matsumoto, D. Kato, R. Ono, H. Kiyama, A. J. Moorhouse, J. Nabekura and H. Wake, *Nat Commun*, 2019, **10**, 5816.

81.   K. Yanagida, C. H. Liu, G. Faraco, S. Galvani, H. K. Smith, N. Burg, J. Anrather, T. Sanchez, C. Iadecola and T. Hla, *Proc Natl Acad Sci U S A*, 2017, **114**, 4531-4536.

82.   S. Yang, C. Gu, E. T. Mandeville, Y. Dong, E. Esposito, Y. Zhang, G. Yang, Y. Shen, X. Fu, E. H. Lo and Z. Xie, *Front Immunol*, 2017, **8**, 902.

83.   Y. Shin, S. H. Choi, E. Kim, E. Bylykbashi, J. A. Kim, S. Chung, D. Y. Kim, R. D. Kamm and R. E. Tanzi, *Advanced Science*, 2019, **6**, 1900962.

84.   P. M. D. Watson, J. C. Paterson, G. Thom, U. Ginman, S. Lundquist and C. I. Webster, *Bmc Neurosci*, 2013, **14**, 59.

85.   C. Hajal, G. S. Offeddu, Y. Shin, S. Zhang, O. Morozova, D. Hickman, C. G. Knutson and R. D. Kamm, *Nature Protocols*, 2022, **17**, 95-128.

86.   G. D. Vatine, R. Barrile, M. J. Workman, S. Sances, B. K. Barriga, M. Rahnama, S. Barthakur, M. Kasendra, C. Lucchesi, J. Kerns, N. Wen, W. R. Spivia, Z. Chen, J. Van Eyk and C. N. Svendsen, *Cell Stem Cell*, 2019, **24**, 995-1005.e1006.

87.   A. Al Ahmad, M. Gassmann and O. O. Ogunshola, *J Cell Physiol*, 2009, **218**, 612-622.

88.   Z. Sun, C. Gao, D. Gao, R. Sun, W. Li, F. Wang, Y. Wang, H. Cao, G. Zhou, J. Zhang and J. Shang, *Fluids Barriers CNS*, 2021, **18**, 21.

89.   S. Michinaga and Y. Koyama, *Int J Mol Sci*, 2019, **20**.

90.   C. Chapouly, A. Tadesse Argaw, S. Horng, K. Castro, J. Zhang, L. Asp, H. Loo, B. M. Laitman, J. N. Mariani, R. Straus Farber, E. Zaslavsky, G. Nudelman, C. S. Raine and G. R. John, *Brain*, 2015, **138**, 1548-1567.

91.   H. Min, J. Hong, I. H. Cho, Y. H. Jang, H. Lee, D. Kim, S. W. Yu, S. Lee and S. J. Lee, *Mol Brain*, 2015, **8**, 23.

92.   B. Liu and A. H. Neufeld, *Glia*, 2000, **30**, 178-186.

93.   Z. G. Zhang, L. Zhang, S. D. Croll and M. Chopp, *Neuroscience*, 2002, **113**, 683-687.

94.   J. I. Alvarez, A. Dodelet-Devillers, H. Kebir, I. Ifergan, P. J. Fabre, S. Terouz, M. Sabbagh, K. Wosik, L. Bourbonniere, M. Bernard, J. van Horssen, H. E. de Vries, F. Charron and A. Prat, *Science*, 2011, **334**, 1727-1731.

95.   J. G. DeStefano, J. J. Jamieson, R. M. Linville and P. C. Searson, *Fluids and Barriers of the CNS*, 2018, **15**, 32.

96.   S. Nakagawa, M. A. Deli, H. Kawaguchi, T. Shimizudani, T. Shimono, Á. Kittel, K. Tanaka and M. Niwa, *Neurochemistry International*, 2009, **54**, 253-263.

97.   S. Nakagawa, M. A. Deli, S. Nakao, M. Honda, K. Hayashi, R. Nakaoke, Y. Kataoka and M. Niwa, *Cell Mol Neurobiol*, 2007, **27**, 687-694.

98.   K. Hatherell, P. O. Couraud, I. A. Romero, B. Weksler and G. J. Pilkington, *J Neurosci Methods*, 2011, **199**, 223-229.

99.   L. B. Thomsen, A. Burkhart and T. Moos, *PLOS ONE*, 2015, **10**, e0134765.

100.   M. A. Erickson and W. A. Banks, *Pharmacological Reviews*, 2018, **70**, 278-314.

101.   B. Elbakary and R. K. S. Badhan, *Scientific Reports*, 2020, **10**.

102.   B. J. Deore, P. P. Partyka, F. Fan and P. A. Galie, *The FASEB Journal*, 2022, **36**.

103.   L. Cucullo, M. Hossain, V. Puvenna, N. Marchi and D. Janigro, *BMC Neurosci*, 2011, **12**, 40.

104.   E. Rahbar, J. C. Cardenas, G. Baimukanova, B. Usadi, R. Bruhn, S. Pati, S. R. Ostrowski, P. I. Johansson, J. B. Holcomb and C. E. Wade, *J Transl Med*, 2015, **13**, 117.

105.   C. J. Zuurbier, C. Demirci, A. Koeman, H. Vink and C. Ince, *J Appl Physiol (1985)*, 2005, **99**, 1471-1476.

106.   L. N. Broekhuizen, B. A. Lemkes, H. L. Mooij, M. C. Meuwese, H. Verberne, F. Holleman, R. O. Schlingemann, M. Nieuwdorp, E. S. Stroes and H. Vink, *Diabetologia*, 2010, **53**, 2646-2655.

107.   Y. Matsukawa, V. H. Lee, E. D. Crandall and K. J. Kim, *J Pharm Sci*, 1997, **86**, 305-309.

108.   V. M. Pulgar, *Front Neurosci*, 2018, **12**, 1019.

109.   N. Muradashvili, R. Tyagi and D. Lominadze, *Front Physiol*, 2012, **3**, 166.

110.   D. J. Begley, *Curr Pharm Des*, 2004, **10**, 1295-1312.

111.   T. Osada, Y. H. Gu, M. Kanazawa, Y. Tsubota, B. T. Hawkins, M. Spatz, R. Milner and G. J. del Zoppo, *J Cereb Blood Flow Metab*, 2011, **31**, 1972-1985.

112.   D. Yeung, J. L. Manias, D. J. Stewart and S. Nag, *Acta Neuropathol*, 2008, **115**, 635-642.

113.   L. M. Cancel, E. E. Ebong, S. Mensah, C. Hirschberg and J. M. Tarbell, *Atherosclerosis*, 2016, **252**, 136-146.

114.   E. E. Ebong, S. V. Lopez-Quintero, V. Rizzo, D. C. Spray and J. M. Tarbell, *Integrative Biology*, 2014, **6**, 338-347.

115.   R. Haeren, S. van de Ven, M. van Zandvoort, H. Vink, J. van Overbeeke, G. Hoogland and K. Rijkers, *Current neurovascular research*, 2016.

116.   I. C. Harding, R. Mitra, S. A. Mensah, A. Nersesyan, N. N. Bal and E. E. Ebong, *Biorheology*, 2019, **56**, 131-149.

117.   R. Booth and H. Kim, *Annals of Biomedical Engineering*, 2014, **42**, 2379-2391.

118.   A. Kamiya and T. Togawa, *American Journal of Physiology-Heart and Circulatory Physiology*, 1980, **239**, H14-H21.

119.   S. Y. Desai, M. Marroni, L. Cucullo, L. Krizanac-Bengez, M. R. Mayberg, M. T. Hossain, G. G. Grant and D. Janigro, *Endothelium*, 2002, **9**, 89-102.

120.   L. Cucullo, B. Aumayr, E. Rapp and D. Janigro, *Curr Opin Drug Discov Devel*, 2005, **8**, 89-99.

121.   A. G. Koutsiaris, S. V. Tachmitzi, N. Batis, M. G. Kotoula, C. H. Karabatsas, E. Tsironi and D. Z. Chatzoulis, *Biorheology*, 2007, **44**, 375-386.
122.   M. W. Van Der Helm, A. D. Van Der Meer, J. C. T. Eijkel, A. Van Den Berg and L. I. Segerink, *Tissue Barriers*, 2016, **4**, e1142493.
123.   N. Choublier, Y. Müller, L. Gomez Baisac, J. Laedermann, C. De Rham, X. Declèves and A. Roux, *Applied Sciences*, 2021, **11**, 5584.